

AD-A244 060



EMI (2)

DTIC  
ELECTE  
DEC 30 1991  
S D

10/91

Viscous Modeling of  
the Interior Ballistic Cycle

R. Heiser

This document has been approved  
for public release and sale; its  
distribution is unlimited.

91-19180



Expl-Nr

6028

91 1227 052

Fraunhofer-Gesellschaft



10 / 91

# VISCOUS MODELING OF THE INTERIOR BALLISTIC CYCLE

R. Heiser

Weil am Rhein, October 1991

Accession For	
NTIS CRASI	<input checked="" type="checkbox"/>
DTIC TAB	<input type="checkbox"/>
Unannounced	<input type="checkbox"/>
Justification	
By	
Distribution /	
Availability Codes	
Dist	Avail and/or Special
A-1	



68 Seiten mit  
41 Abbildungen  
17 Literaturstellen

REPORT DOCUMENTATION PAGE

1a. REPORT SECURITY CLASSIFICATION Unclassified		1b. RESTRICTIVE MARKINGS	
2a. SECURITY CLASSIFICATION AUTHORITY		3. DISTRIBUTION/AVAILABILITY OF REPORT Approved for public release; distribution unlimited	
2b. DECLASSIFICATION/DOWNGRADING SCHEDULE			
4. PERFORMING ORGANIZATION REPORT NUMBER(S)		5. MONITORING ORGANIZATION REPORT NUMBER(S) R&D 5330-AN-01	
6a. NAME OF PERFORMING ORGANIZATION Ernst-Mach-Institut	6b. OFFICE SYMBOL (if applicable)	7a. NAME OF MONITORING ORGANIZATION European Research Office USARDSG-UK	
6c. ADDRESS (City, State, and ZIP Code) Fraunhofer-Institut fur Kurzzeitdynamik, Institutsteil Weil Am Rhein, Postfach 1270, D7858 Weil Am Rhein, Germany		7b. ADDRESS (City, State, and ZIP Code) Box 65 FPO NY 09510-1500	
8a. NAME OF FUNDING/SPONSORING ORGANIZATION European Research Office USARDSG-UK ARO-E	8b. OFFICE SYMBOL (if applicable)	9. PROCUREMENT INSTRUMENT IDENTIFICATION NUMBER DAJA45-86-C-0031	
8c. ADDRESS (City, State, and ZIP Code) Box 65 FPO NY 09510-1500		10. SOURCE OF FUNDING NUMBERS	
		PROGRAM ELEMENT NO. 61102A	PROJECT NO. iL161102BH7
		TASK NO. 06	WORK UNIT ACCESSION NO.
11. TITLE (Include Security Classification) (U) Viscous Modeling of the Interior Ballistic Cycle			
12. PERSONAL AUTHOR(S) Dr. R. Heiser			
13a. TYPE OF REPORT Final	13b. TIME COVERED FROM Apr. 87 TO May 91	14. DATE OF REPORT (Year, Month, Day) 1991, October, 18	15. PAGE COUNT 68
16. SUPPLEMENTARY NOTATION			
17. COSATI CODES		18. SUBJECT TERMS (Continue on reverse if necessary and identify by block number)	
FIELD	GROUP	Viscous Flow, Navier-Stokes Equations, Turbulence, Heat Transfer, Boundary Layer	
19. ABSTRACT (Continue on reverse if necessary and identify by block number)			
<p>The propellant gas flow behind a projectile inside of a tube weapon is investigated numerically. The main subject is coupled to the viscosity related phenomena such as boundary layer formation, turbulence and heat transfer to the wall. Therefore, the full Navier-Stokes equations are used to describe the gas flow. Different kinds of turbulence models are implemented. Comparisons with experimental results are performed. The DELTA code is used as the basis for the numerical simulation and extended properly for turbulence and heat transfer. Several numerical results are presented. Fundamental thoughts on the numerics are added.</p>			
20. DISTRIBUTION/AVAILABILITY OF ABSTRACT <input checked="" type="checkbox"/> UNCLASSIFIED/UNLIMITED <input checked="" type="checkbox"/> SAME AS RPT. <input checked="" type="checkbox"/> DTIC USERS		21. ABSTRACT SECURITY CLASSIFICATION Unclassified	
22a. NAME OF RESPONSIBLE INDIVIDUAL Dr. R. Reichenbach		22b. TELEPHONE (Include Area Code) 071 409 4423/4485	22c. OFFICE SYMBOL AMXSN-UK-RA

## Table of Contents

	<u>Page</u>
Introduction	4
Numerical Techniques	5
Turbulence	5
Heat Transfer	7
Numerical Results	8
Conclusions	12
References	13
Figures	16
Appendix: Interior Ballistics and Gun Barrel Heat Transfer by S. C. Kocaaydin	57

## **Introduction**

During the interior ballistic cycle in conventional tube weapons, processes of different importance occur. The most important process, the motion of the projectile, depends on the burning of the propellant and thus the generation of gas pressure in the gun. The interior ballisticians however know, that beside this key process a series of further processes must be considered, limiting the design of a charge. Important points of view are for instance the life-time of gun tubes, which is coupled to the erosion, or the cook-off of charges. These examples show that the generation of heat and heat transport processes play an important role. The heat transport processes of heat conduction, convection and radiation as well as heat transfer should be considered.

It is the subject of this contract, to explore the heat transport processes in interior ballistic flows by means of numerical simulation. The numerical simulation for high velocity flows under high pressure and high temperature should be limited however to pure gas flows behind a projectile. The general subject of the contract "Viscous Modeling of the Interior Ballistic Cycle" emphasizes the viscosity of the interior ballistics gas flow to be included. The viscosity of the flow is taken into consideration by using the full Navier-Stokes equations for describing a multidimensional (axisymmetric) unsteady and compressible flow. This kind of mathematical description opens the possibility of calculating the formation of the boundary layer, which is important for the heat transfer and for including turbulence as an essential process for the heat convection. Actually, this kind of simulation considers the complete coupling of the flow between the core and the transient boundary layer as well as the interaction of the heat transfer into the tube wall and the wall. This report gives account of the achieved results of the numerical simulation. The comparisons between laminar and turbulent flow have been published already at other places, among others in six periodic reports, and therefore are presented here only in summary. The investigation of the heat transfer to the tube wall, however, is treated more comprehensively.

Substantial work on this contract has been performed by the Research Associates

Dr. J. Garloff (Apr 87 - March 89) and  
Dr. S. Kocaaydin (June 90 - May 91).

Mr. K. Wolf has been responsible for the graphic evaluation of the tremendous amount of computational results. The financial support provided by the U.S. Army Ballistic Research Laboratory, Aberdeen Proving Ground, Maryland, through the U.S. Army European Research Office, London, is acknowledged.

### **Numerical Techniques**

For the numerical solution of the Navier-Stokes equations the DELTA-Code was available. Originally, this computer code was supposed to provide a numerical approximation of the solution of the averaged two-phase (gas-solid), multi-dimensional equations governing viscous interior ballistic flows within conventional guns [1,2]. The numerical method is based on a linearized Alternating Direction Implicit (ADI) scheme of the Briley-McDonald type [3] and applied to a moving coordinate system caused by the moving projectile. The implicit finite difference method is very well suited, since a satisfactory resolution of the boundary layer makes necessary very small grids in the wall proximity. To keep the amount of grid points as small as possible a distribution of nonequidistant grids is used in radial direction with most narrow grids at the wall and increasing grid size in direction to the tube axis. In axial direction equidistant grids were sufficient. The code was developed at the BRL on a CDC mainframe computer in UPDATE format. At the time DELTA was transferred to the VAX computers accessible to the Ernst-Mach-Institut (EMI), only those code modules for an axisymmetric laminar gas flow for adiabatic walls had been tested. Beside the main program the graphics package based on DISSPLA also was installed on the EMI-computer for processing the numerical results. The graphic was extended substantially to make possible a sufficient monitoring of the computer runs and a postprocessing.

### **Turbulence**

Computational results for the laminar interior ballistic gas flow showed very thin boundary layers [4] for the axial flow velocity as well as for the gas temperature. By comparing the experimental results from ballistic simulators [5,6,7] to the computational results of the laminar flow, differences appeared for the shape of the velocity boundary layer even for low velocities. The measured velocity traces pointed to turbulence as the source of the differences.

In a first step we studied the applicability of two algebraic eddy viscosity models of turbulence using a two-layer approach since their implementation did not cause too many modifications in the code. Both the Cebeci-Smith-Mosinskis model and the Baldwin-Lomax model did not generate realistic turbulent flow profiles in the boundary layer. However the boundary layer thickness (99 % criterion) looked similar to the experimental results. Although performing an extensive parameter analysis we did not get satisfying results when comparing with the experimental results with the gun simulators of the Imperial College, London [5,6]. In order to describe adequately the heat transfer it is necessary to start from realistic boundary layer profiles. The results using the algebraic turbulence models were published in detail [8-12].

The experience with the algebraic models of turbulence caused us to incorporate a more advanced turbulence model based on transport equations for turbulent quantities. As next step we modified the widely used  $k-\epsilon$  model taking into consideration compressibility effects [13]. Special emphasis was laid on the modeling of pressure-velocity correlations appearing in the equation for internal energy as well as turbulent kinetic energy  $k$ . This model was strictly extended in order to include real gas effects (Noble-Abel equation of state) and to facilitate the investigations on heat transfer. Then the  $k-\epsilon$  model was implemented in the DELTA code. Test runs showed that the values of the turbulent kinetic dissipation rate rose too fast in the corner between the projectile base and the tube wall.

In view of the numerical difficulties with the  $k-\epsilon$  model a one-equation model was considered as a more appropriate candidate. This equation is a transport equation for the turbulent kinetic energy. Its dissipation rate is given by means of a mixing length specified algebraically. By applying this model in DELTA we achieved reasonable computational results in good agreement with the experimental ones. The basic equations as well as the comparison with the experiments are documented in [11,12].

## Heat Transfer

Besides the modeling of turbulent gas flow close to the wall the calculation of the heat transfer from the hot propellant gases to the tube wall was a further important goal of this contract. Two ways of solution were traced. First, the boundary condition at the wall surface was formulated as a heat balance. Second, a finite volume formulation was chosen such that a volume across the boundary includes a part of the flow and of the wall. This method is described in detail by C. S. Kocaaydin in the Appendix of this report whereas the first method is explained in the following. Both methods required substantial extensions of the DELTA code as well as of the graphics for postprocessing and consequently plenty of coding.

In order to calculate the heat transfer to the tube the boundary condition used so far for an adiabatic wall surface was changed such that the heat exchange between flow and wall is described. In this case both the heat flux from the hot gas and the quantity of radiated heat to the wall are supposed to equal the heat flux penetrating into the wall:

$$-\lambda_g \frac{\partial T_g}{\partial r} + \epsilon \sigma (T_{g0}^4 - T_g^4) = -\lambda_w \frac{\partial T_w}{\partial r}$$

and on the inner tube surface the gas temperature  $T_g$  is supposed to equal the wall temperature  $T_w$ :

$$T_g = T_w$$

The variables  $\lambda$ ,  $\epsilon$ ,  $\sigma$  and  $r$  denote the thermal conductivity, the emissivity of the wall surface, the Stefan-Boltzmann constant and the radial coordinate, respectively. The index  $g$  stands for gas, and  $w$  for wall. The temperature  $T_{g0}$  means the maximum gas temperature in a particular cross-section of the tube. In the wall the two-dimensional heat conduction equation

$$\rho_w c_w \frac{\partial T_w}{\partial t} = \frac{\partial}{\partial z} \left( \lambda_w \frac{\partial T_w}{\partial z} \right) + \frac{1}{r} \frac{\partial}{\partial r} \left( r \lambda_w \frac{\partial T_w}{\partial r} \right)$$

is solved using the same numerical scheme as for the gas flow region.  $\rho$ ,  $c$ ,  $t$ ,  $z$  denote the density and specific heat of the wall material, time and axial coordinate in the wall, respectively. At the outer tube wall surface the simple engineering condition

$$-\lambda_w \frac{\partial T_w}{\partial r} = h (T_w - T_{amb})$$

is chosen where we are using a heat transfer number  $h$  and an outer ambient temperature  $T_{amb}$ . A more sophisticated condition, at least for a single shot weapon, is not necessary because the heat usually does not reach the outer surface during the ballistic cycle because of the wall thickness. Two additional boundary conditions are needed in axial direction for the heat conduction equation. At the projectile base, we set

$$T_w = T_{amb}$$

across the wall thickness, that is, we assume the projectile moves into a cold area with ambient temperature. This assumption is not true if there is a gas leakage around the projectile. At the breech, an adiabatic condition

$$\frac{\partial T_w}{\partial z} = 0$$

seems to be adequate.

### Numerical Results

In the following numerical results will be presented. In order to avoid an initial discontinuity in temperature at the wall surface the initial temperature is assumed to be ambient everywhere in the flow area and in the wall. Also, the initial pressure is ambient. For producing a time-dependent pressure and temperature profile as in a real tube weapon, mass and energy are added to the one-phase flow via source terms. These source terms take into account an empirical burning law as a function of pressure. The sources move with the flow. A constant time-step of  $10 \mu s$  was chosen. The computational mesh consists of 97 uniformly spaced grid points in the axial direction and 73 nonuniformly spaced grid points in the radial direction for the gas flow whereas 73 uniformly spaced grid points are used in the wall in radial direction.

Table 1. Parameters of the Test Run

Bore Diameter	20 mm
Tube Length (Breech to Muzzle)	2.0 m
Initial Chamber Length	0.175 m
Projectile Mass	120 g
Ratio of Specific Heats	1.271
Covolume	$1.08 \cdot 10^{-3} \text{ m}^3/\text{kg}$
Molar Mass	23.8 g/mole
Barrel Material	Steel 4130
Density	$7800 \text{ kg/m}^3$
Thermal Conductivity	43 W/m/K
Specific heat	460 J/kg/K
Emissivity Factor	0.7
Initial Gas Pressure	0.1 MPa
Initial Gas and Wall Temperature	293 K
Initial Gas Velocity	0 m/s
Shot Start Pressure	0.1 MPa

The smallest grid size in radial direction is  $0.61 \mu\text{m}$  on the gas side and  $34.7 \mu\text{m}$  in the wall. Other parameters for this test run are summarized in Table 1. Several Figures referring to the boundary layer, wall temperature distribution, heat transfer, spatial distribution of flow quantities and projectile motion will be presented. 5.81 ms after the beginning of the shot cycle the projectile leaves the muzzle with the velocity of 941 m/s having run a distance of 1.825 m down the tube. Bore friction is neglected.

Figures 1 to 3 show information on the projectile motion. Pressure as well as temperature rise and drop versus time are displayed in Figures 4 and 5, respectively. As mentioned before mass and energy is added to the flow in order to achieve realistic gas and temperature profiles. This is based on a hypothetical mass of propellant the consumption of which is shown in Figure 6. The spatial distribution of the axial flow velocity, radial flow velocity and gas pressure are plotted in Figures 7 to 9, respectively, for the time of muzzle clearance. At this time the boundary layer in the front part behind the projectile is fully developed (cf. Fig. 7). The turbulent kinetic energy and the Reynolds stress are shown in Figures 10 and 11, respectively.

In Figure 12 the temperature distribution in the gas and in the wall are given for the same time. The wall surface is the line where the red and green areas meet each other. The wall temperature is resolved more detailed in Figure 13. Temperature measurements are taken at fixed locations along the wall. Therefore, the Figures 14 to 16 show at the positions 100, 200 and 300 mm off the breech the temperature curves for the wall surface and for the depths in the wall of 10, 30, 50, 100  $\mu\text{m}$ . One has to keep in mind that the initial position of the projectile is 175 mm off the breech. The wall temperature depends on the heat flux. The heat, transferred from the hot gas to the cool wall along the tube is integrated over time in Figure 17. The decrease of the transferred heat from the maximum at about 200 mm is caused by the decrease in heat convection when approaching to the breech. The convection of heat is supposed to be the dominant heat transport process to the wall in order to feed the gas layer next to the wall with heat. This is one of the most interesting results of this heat transfer study.

Several additional figures illustrate some other features of the viscous flow solution. Next, the development of the velocity boundary layer (99 % criterion) is shown in a sequence of plots in Figures 18 to 22. For the time of muzzle clearance the radial profiles of the axial flow velocity, radial flow velocity and gas and wall temperature are displayed occurring 0.5, 1.5 and 1.95 m off the breech. This concludes the presentation of numerical results for the particular 20-mm test example. Of course there exist many other interesting results. The figures and explanations given here are supposed to represent the most important attributes of the viscous turbulent interior ballistics one-phase flow with heat transfer.

As another test example the 22.2 mm experimental gun simulator of the Imperial College was chosen. The essential parameters of this test rig are given in Table 2. The gas used is low grade nitrogen. The flow is a pure expansion flow starting from the initial gas pressure of 1.1 MPa behind the projectile. This example has been used for an extensive comparison of the particular flow characteristics between experiment and numerical simulation. Above all the modeling of the turbulence was verified. Since those results have been published in Refs. 10 to 12 only the heat transfer results are presented in the following. They are referred to the Figures 32 to 41. The computational mesh again uses 97 x 73 grid points. Figures 32 to 34 show the projectile motion. Because of the low initial pressure the achieved maximum velocity is only about 200 m/s.

**Table 2. Parameters of the gun simulator**

<b>Bore Diameter</b>	<b>22.2 mm</b>
<b>Tube Length (Breech to Muzzle)</b>	<b>3.56 m</b>
<b>Initial Chamber Length</b>	<b>1.3 m</b>
<b>Projectile Mass</b>	<b>10.5 g</b>
<b>Ratio of Specific Heats</b>	<b>1.416</b>
<b>Covolume</b>	<b>0 m<sup>3</sup>/kg</b>
<b>Molar Mass</b>	<b>28.0 g/mole</b>

**Barrel Material and Properties as in Table 1**

<b>Initial Gas Pressure</b>	<b>1.1 MPa</b>
<b>Initial Gas and Wall Temperature</b>	<b>293 K</b>
<b>Initial Gas Velocity</b>	<b>0 m/s</b>
<b>Shot Start Pressure</b>	<b>0.1 MPa</b>

The pressure as well as the temperature drop both at the projectile base and breech according to the expansion are plotted in the Figures 35 and 36. Since the expansion starts from ambient temperature the gas temperature drops below the ambient temperature. This means heat is transferred from the wall to the flow as shown in the Figures 37 to 40 where the wall temperature at the locations 1.0, 1.2, 1.5 and 2.0 off the breech are shown for the wall surface and the wall depths of 10, 30, 50 and 100  $\mu\text{m}$ . The integral heat flux (cf. Fig. 41), therefore, is negative. The computed temperature drops in the wall, however, is not in agreement with those experimental results published in Ref. [7]. There, the measured temperature decreases about 4 to 6  $^{\circ}\text{C}$  whereas the computed temperature decreases about 1  $^{\circ}\text{C}$  or less. The reasons for the difference are not known at this writing.

## Conclusions

The Navier-Stokes solution is able to predict particular flow features of a one-phase interior ballistic flow such as boundary layer, turbulence or heat transport. A one-equation model of turbulence seems to be best suited to incorporate turbulence important to generate the proper amount of heat convection. Another satisfying result concerns the success in calculating the rise of temperature in the tube wall.

Some of the numerical results need to be verified experimentally above all in the high velocity regime. An extension of the study to the application of this mathematical model on two-phase flows with inert and reactive solid particles is recommended.

## References

### General

- [1] A.K.R. Celmins, J.A. Schmitt  
"Volume Averaged Two-Phase (Gas Solid) Interior Ballistics Equations"  
BRL Technical Report TR-2593, Sept. 1984
- [2] J.A. Schmitt  
"A Numerical Algorithm for the Multidimensional Multiphase, Viscous Equations of Interior Ballistics"  
Transactions of the 2nd Army Conf. on Applied Mathematics and Computing, Troy, NY, May 1984, ARI Report 85-1, 649-691
- [3] W.R. Briley, H. McDonald  
"Solution of the Multidimensional Compressible Navier-Stokes Equation by a Generalized Implicit Method"  
J. Comp. Phys. 24 (1977), 372-397
- [4] R. Heiser, J. Schmitt  
"Simulations of Special Interior Ballistic Phenomena With and Without Heat Transfer to the Gun Tube Wall"  
Transactions of the 2nd Army Conf. on Applied Mathematics and Computing, Troy, NY, May 1984, ARO Report 85-1, 405-457
- [5] A.F. Bicen, L. Khezzar, J.H. Whitelaw  
"Subsonic Single-Phase Flow in a Gun Simulator"  
AIAA J. 25 (1988), 47-51
- [6] M.C. Schmidt  
"A Single-Phase Flow in a High Speed Gun Simulator"  
Imperial College of Science, Technology and Medicine, London, Report FS/89/02, 1989
- [7] A.F. Bicen, J.R. Laker, M.D. Schmidt, J.H. Whitelaw  
"Instrumentation for Transient Gas Velocity, Pressure and Heat Flux Measurements in a Gun Simulator"  
Proceedings 13th International Congress on Instrumentation in Aerospace Simulation Facilities, Göttingen, Germany, September 1989

Reports referring to the contract

- [8] J. Garloff, R. Heiser  
"Ein neuer Anlauf zur Berechnung der reibungsbehafteten innenballistischen Strömung"  
Proceedings 14th Symposium "Innenballistische Leistungssteigerung von Rohrwaffen", BICT, Swisttal-Heimerzheim, 8-10 November 1988
- [9] J. Garloff, R. Heiser  
"Comparison of Two Algebraic Eddy Viscosity Models for Turbulent Modeling of Interior Ballistics Flows"  
Fraunhofer-Institut für Kurzezeitdynamik, Ernst-Mach-Institut, Weil am Rhein, EMI Report 7/88, December 1988
- [10] J. Garloff, R. Heiser  
"A Contribution to the Boundary Layer Development in Interior Ballistic Flows"  
Proceedings 11th International Symposium on Ballistics, Vol. I, Brussels, Belgium, May 1989, pp. 327-336
- [11] J. Garloff, R. Heiser  
"A Contribution to the Turbulence of Interior Ballistics Flows"  
AIAA Paper 89-2557
- [12] R. Heiser, J. Garloff  
"Study on Turbulence in Interior Ballistics Flows"  
Journal of Propulsion and Power to appear in 1991
- [13] J. Garloff, R. Heiser  
"Turbulence Modeling of One-Phase Interior Ballistics Flows by a Two-Equation Model"  
Fraunhofer-Institut für Kurzezeitdynamik, Ernst-Mach-Institut, Weil am Rhein, EMI Report 1/88, March 1988

Presentations referring to the contract

J. Garloff

- BRL-IBD, Aberdeen Proving Ground, September 1987
- ARO Conference on Two-Phase Flow Ernst-Mach-Institut, Weil am Rhein, May 10, 1988

**R. Heiser**

- BRL-IBD, Aberdeen Proving Ground, October 12, 1988
- "A Contribution to the Turbulence of Interior Ballistics Flows"  
AIAA/ASME/SAE/ASEE 25th Joint Propulsion Conference, Monterey, California, July 10-12, 1989
- U.S. Army Workshop "Unsteady and Two-Phase Flow"  
Imperial College of Science, Technology and Medicine, London, England, June 28-29, 1990
- BRL-IBD, Aberdeen Proving Ground, July 24, 1991

**S. Kocaaydin**

- BRL-IBD, Aberdeen Proving Ground, July 11, 1991

# TIME HISTORY

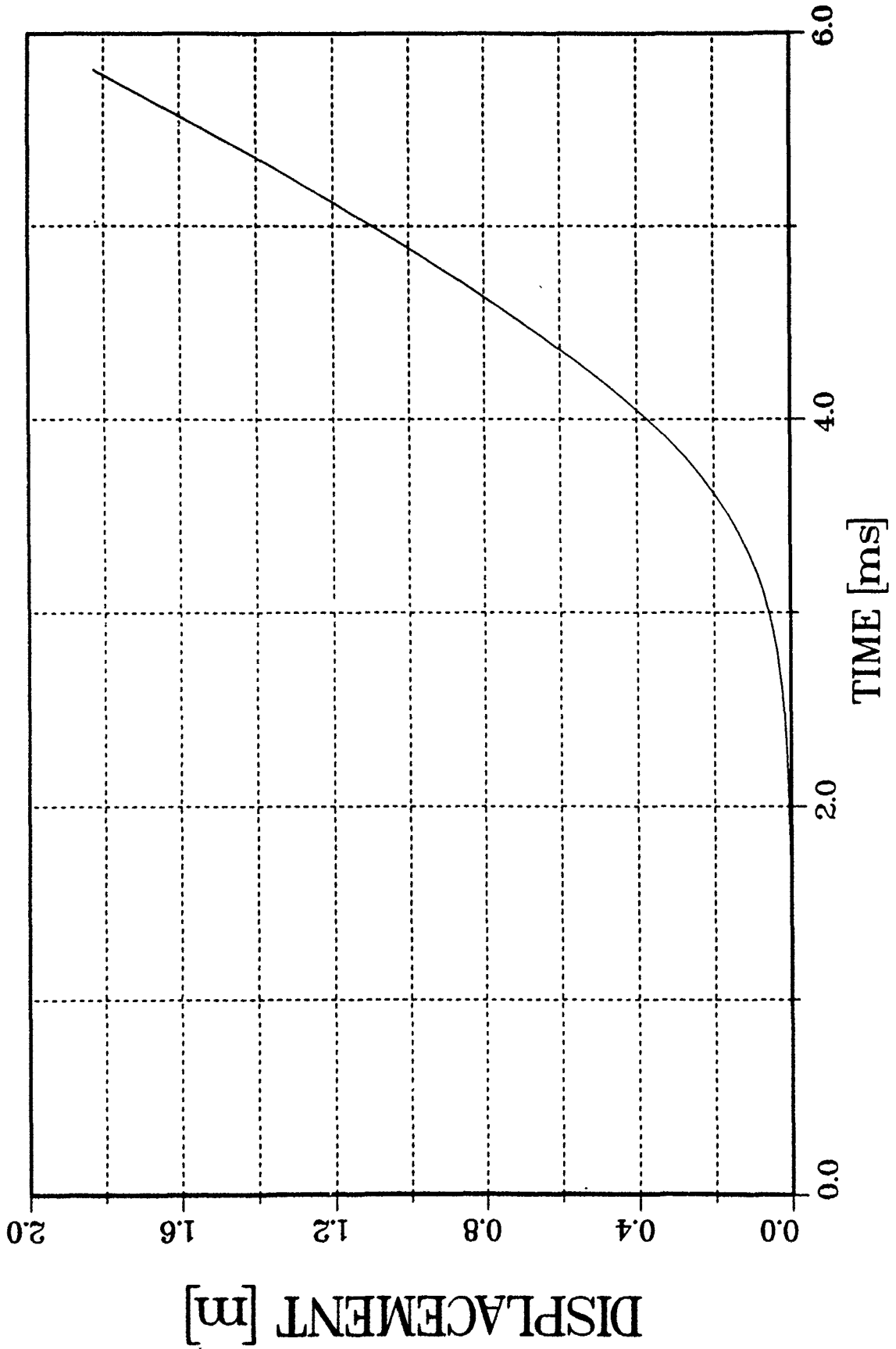


Fig. 1: Projectile displacement versus time

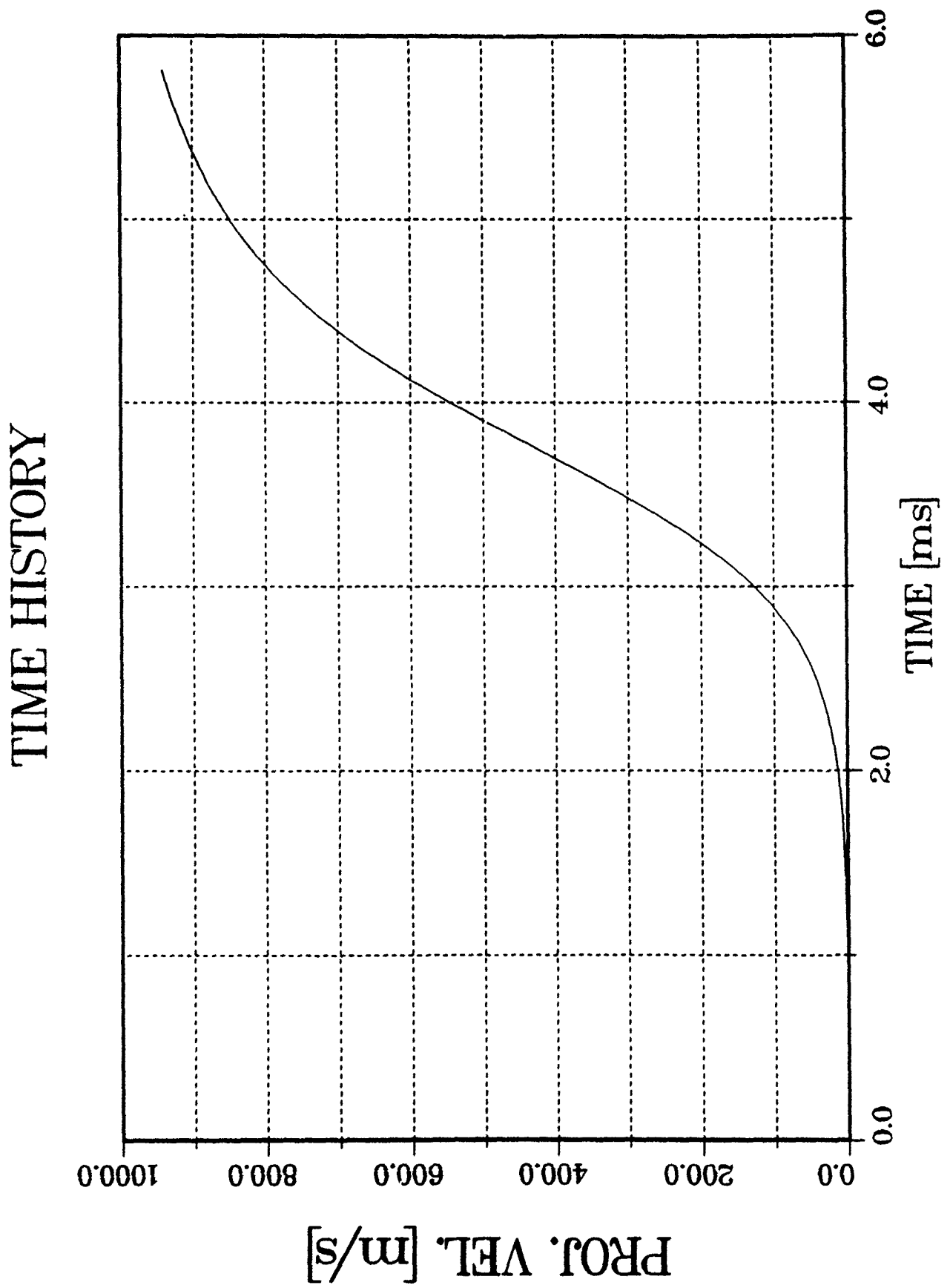


Fig. 2: Projectile velocity versus time

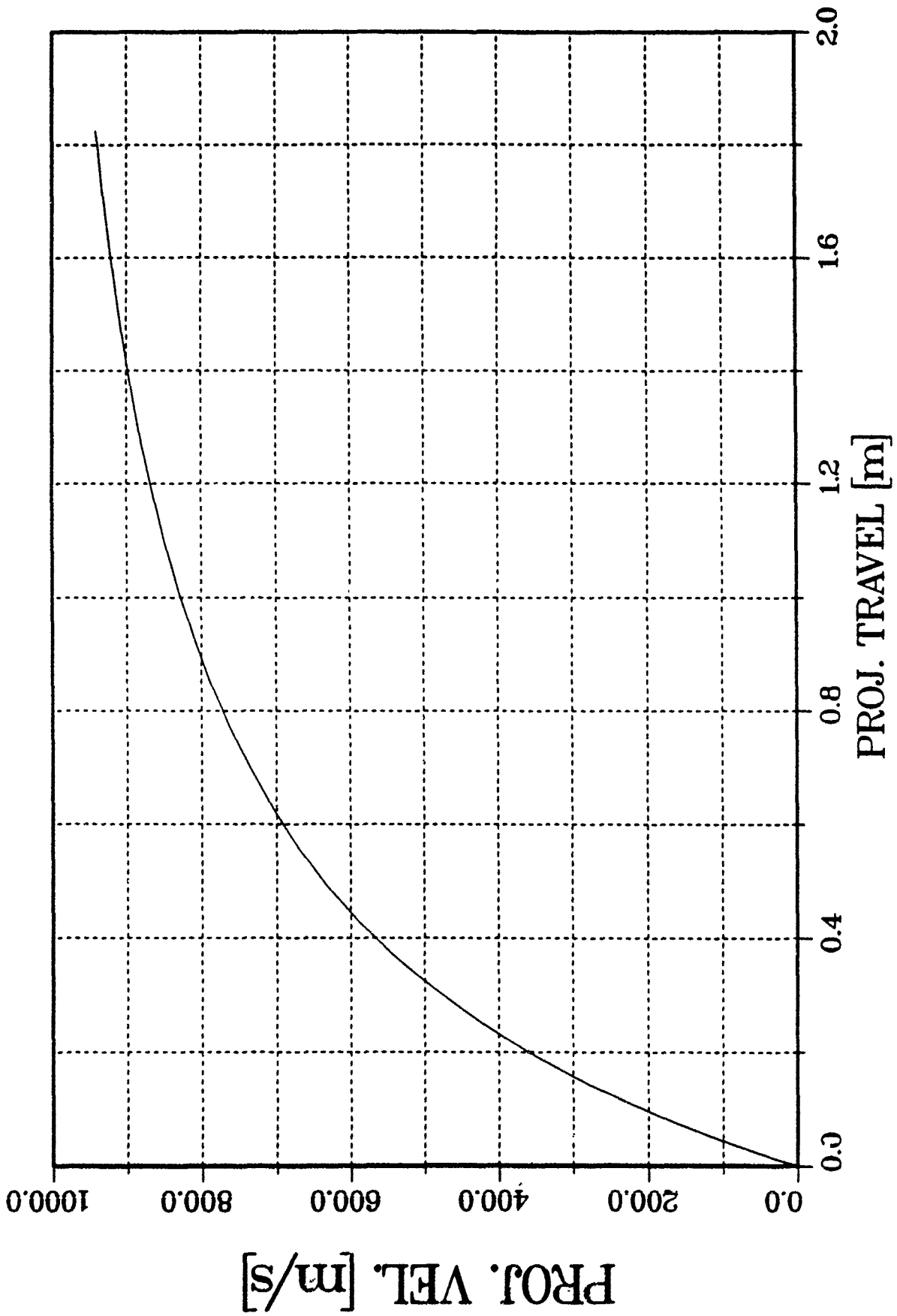


Fig. 3: Projectile velocity versus projectile travel

# TIME HISTORY

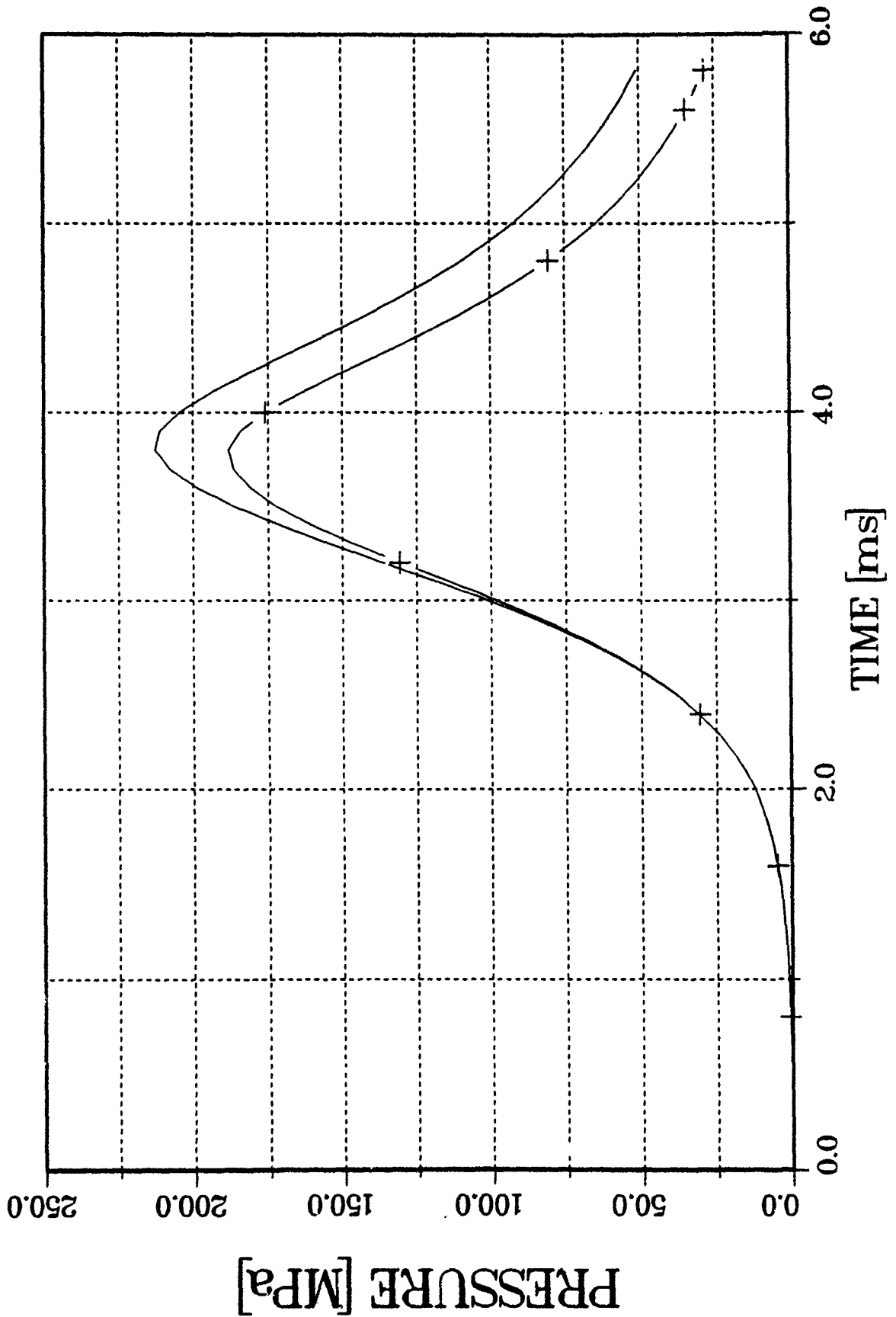


Fig. 4: Gas pressure at the breech and projectile base versus time

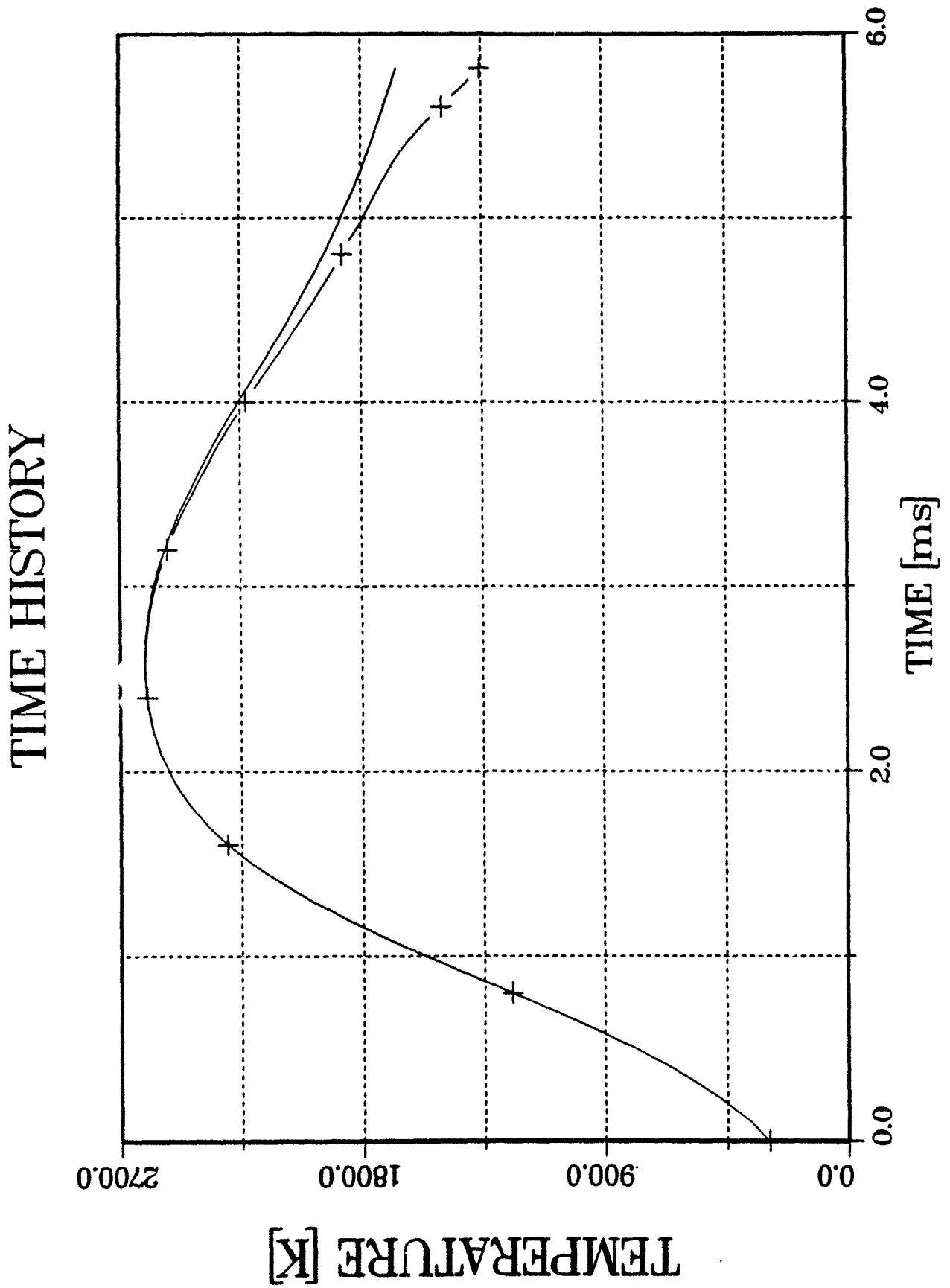


Fig. 5: Gas temperature at the breech and projectile base versus time

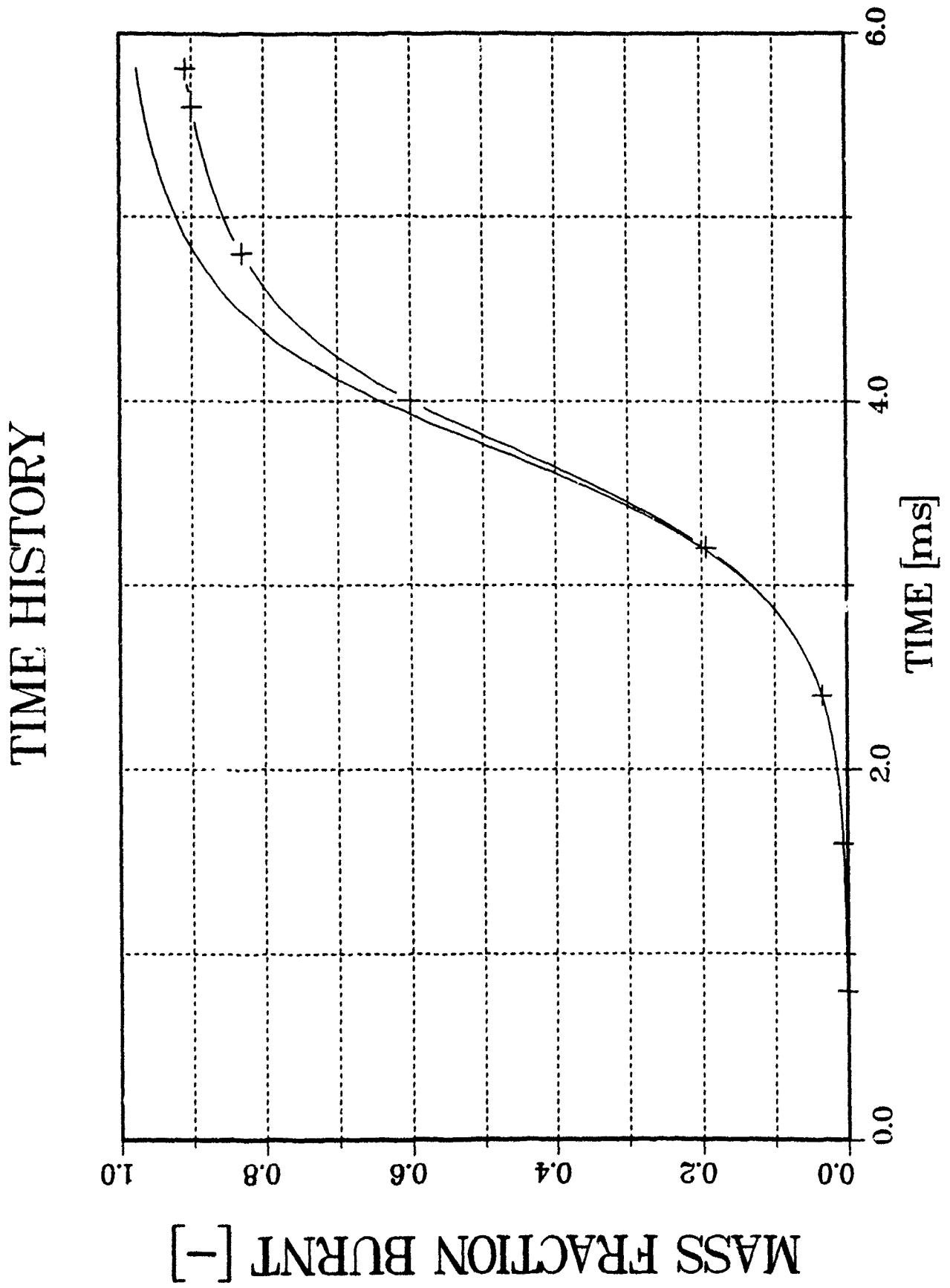


Fig. 6: Hypothetical mass fraction burnt at the breech and projectile base versus time

TIME-STEP= 582    TIME= 5.809 [ms]  
PROJ. DISPLACEMENT=2.000 [m]    PROJ. VEL.= 941 [m/s]

### AXIAL FLOW VEL.

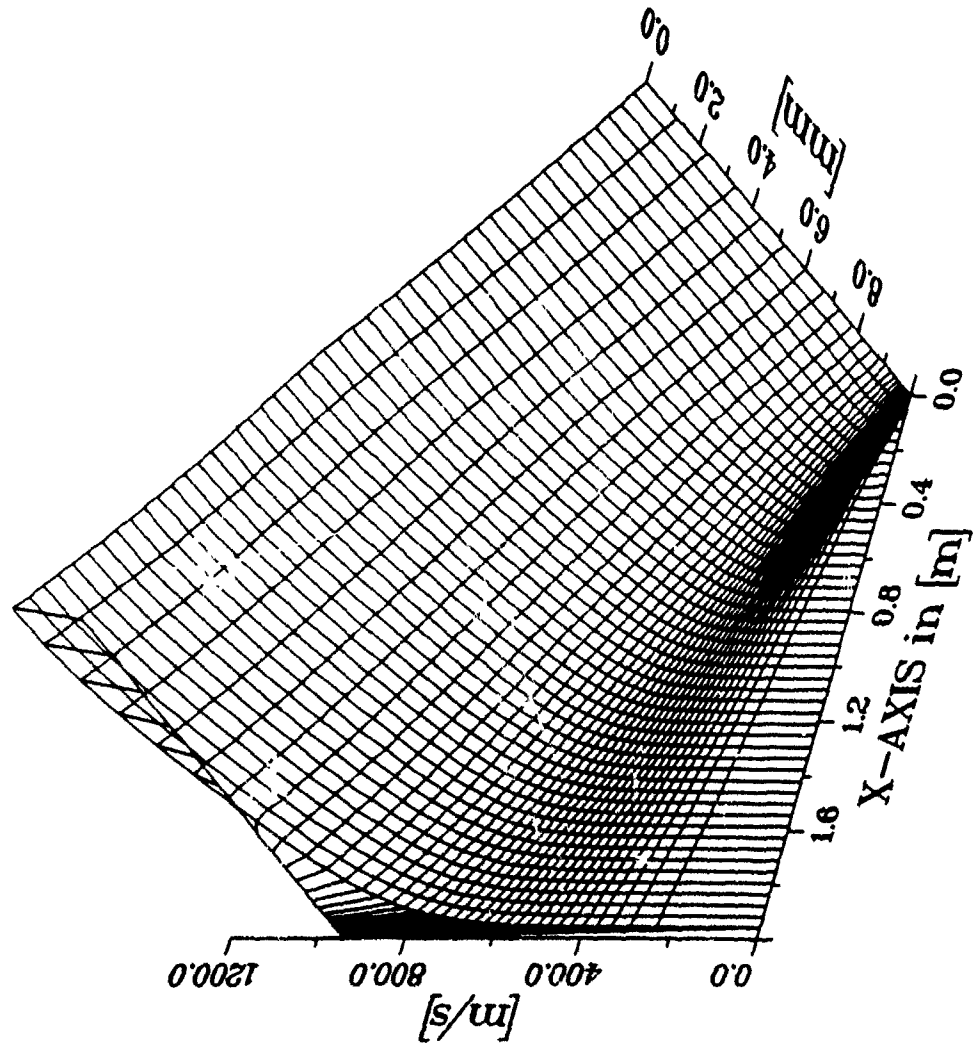
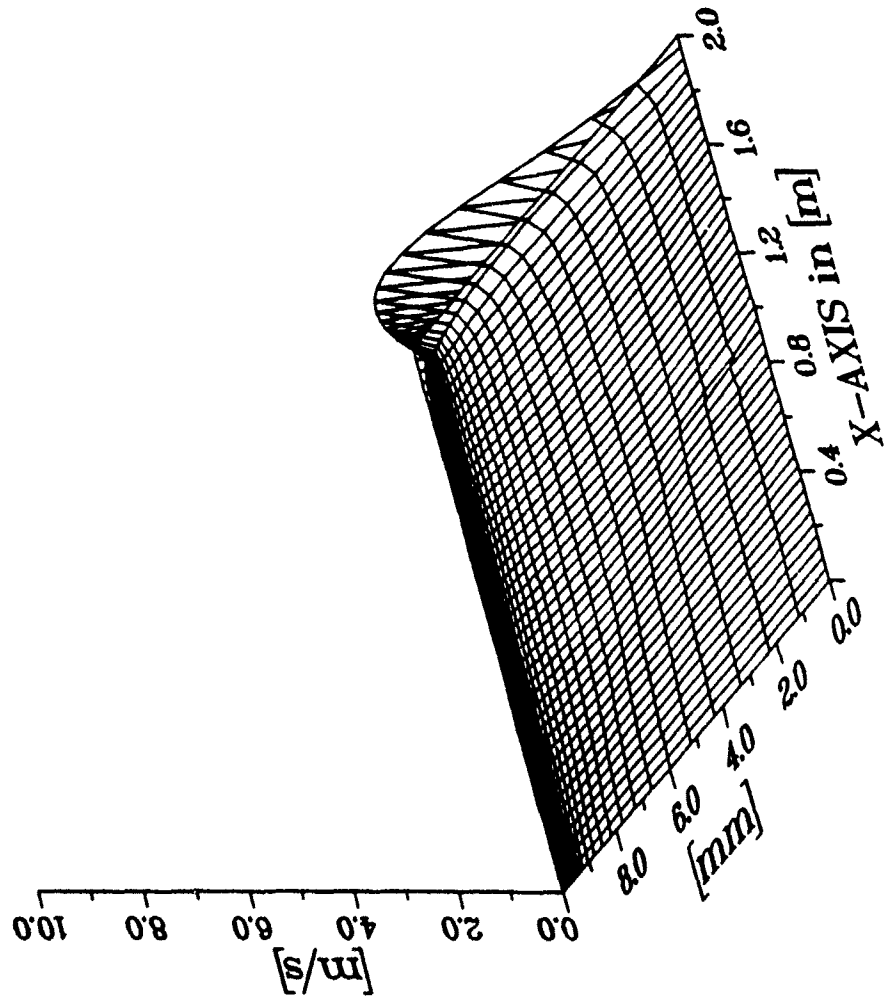


Fig. 7: Axial flow velocity at muzzle clearance

TIME-STEP= 582    TIME= 5.809 [ms]  
PROJ. DISPLACEMENT=2.000 [m]    PROJ. VEL.= 941 [m/s]



### RADIAL FLOW VEL.

Fig. 8: Radial flow velocity at muzzle clearance

TIME-STEP= 582    TIME= 5.809 [ms]  
PROJ. DISPLACEMENT=2.000 [m]    PROJ. VEL.= 941 [m/s]

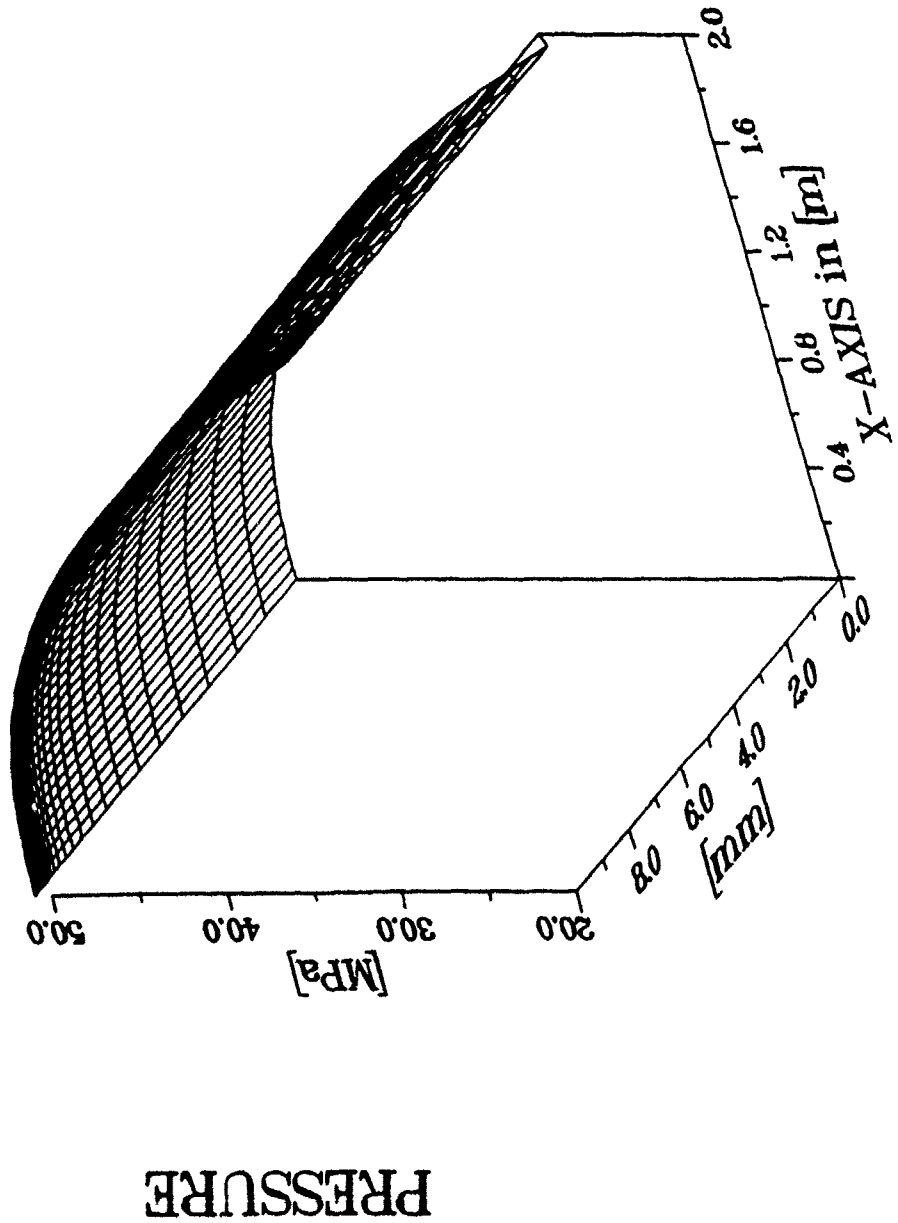
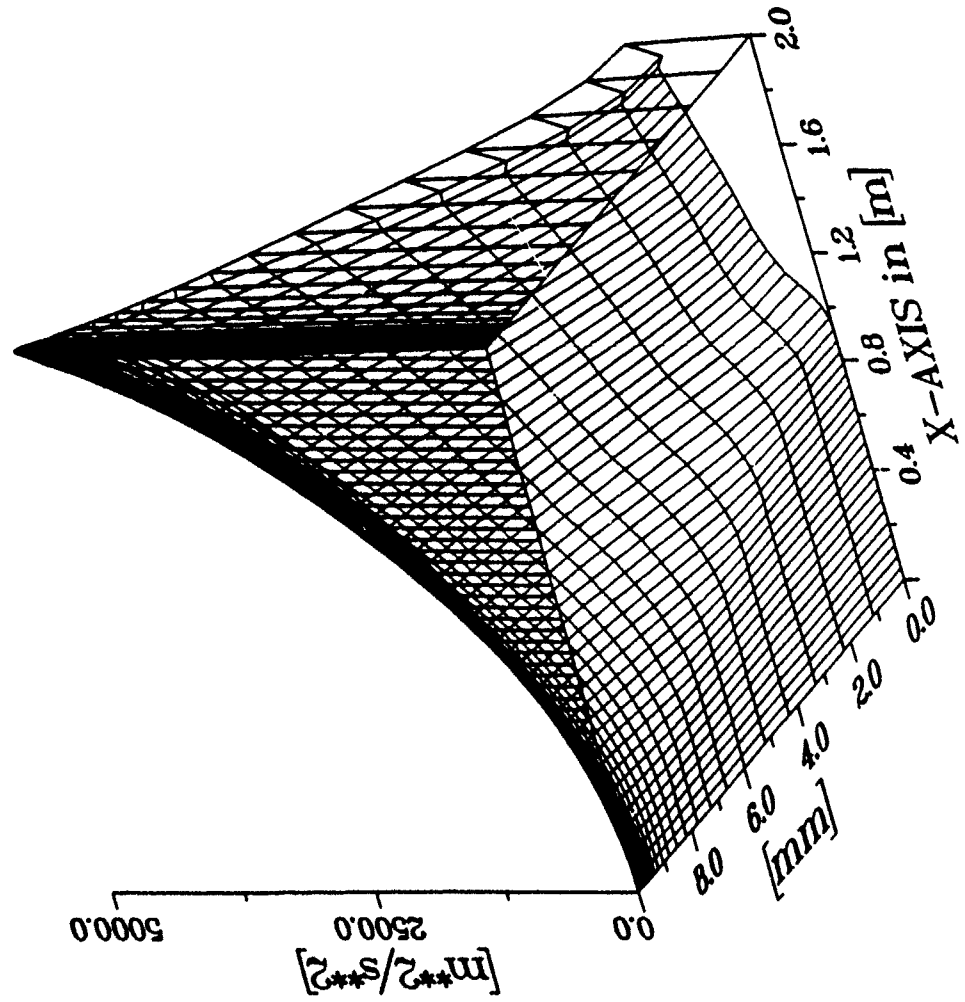


Fig. 9: Gas pressure at muzzle clearance

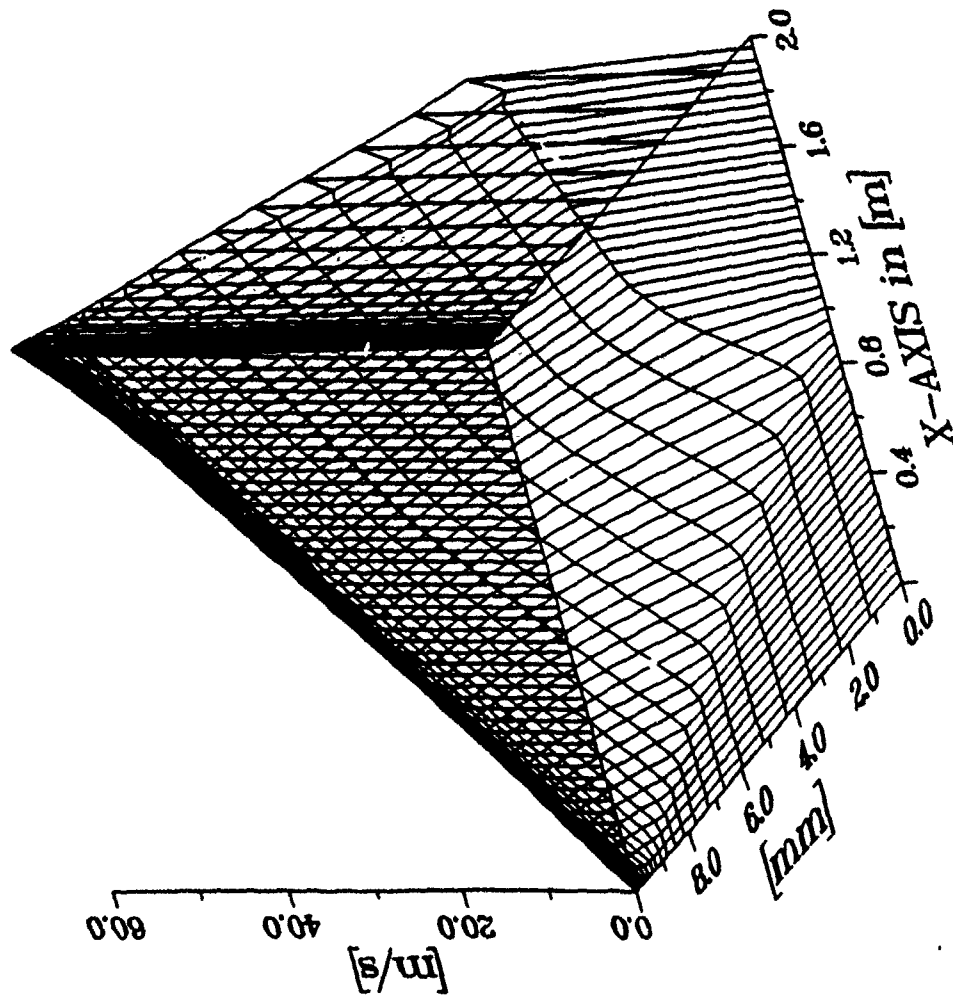
TIME-STEP= 582    TIME= 5.809 [ms]  
PROJ. DISPLACEMENT=2.000 [m]    PROJ. VEL.= 941 [m/s]



TURB. KIN. ENERGY

Fig. 10: Turbulent kinetic energy at muzzle clearance

TIME-STEP= 582    TIME= 5.809[ms]  
PROJ. DISPLACEMENT=2.000[m]    PROJ. VEL.= 941[m/s]



### REYNOLDS STRESS

Fig. 11: Reynolds stress at muzzle clearance

TIME-STEP= 582    TIME= 5.809 [ms]  
PROJ. DISPLACEMENT=2.000 [m]    PROJ. VEL.= 941 [m/s]

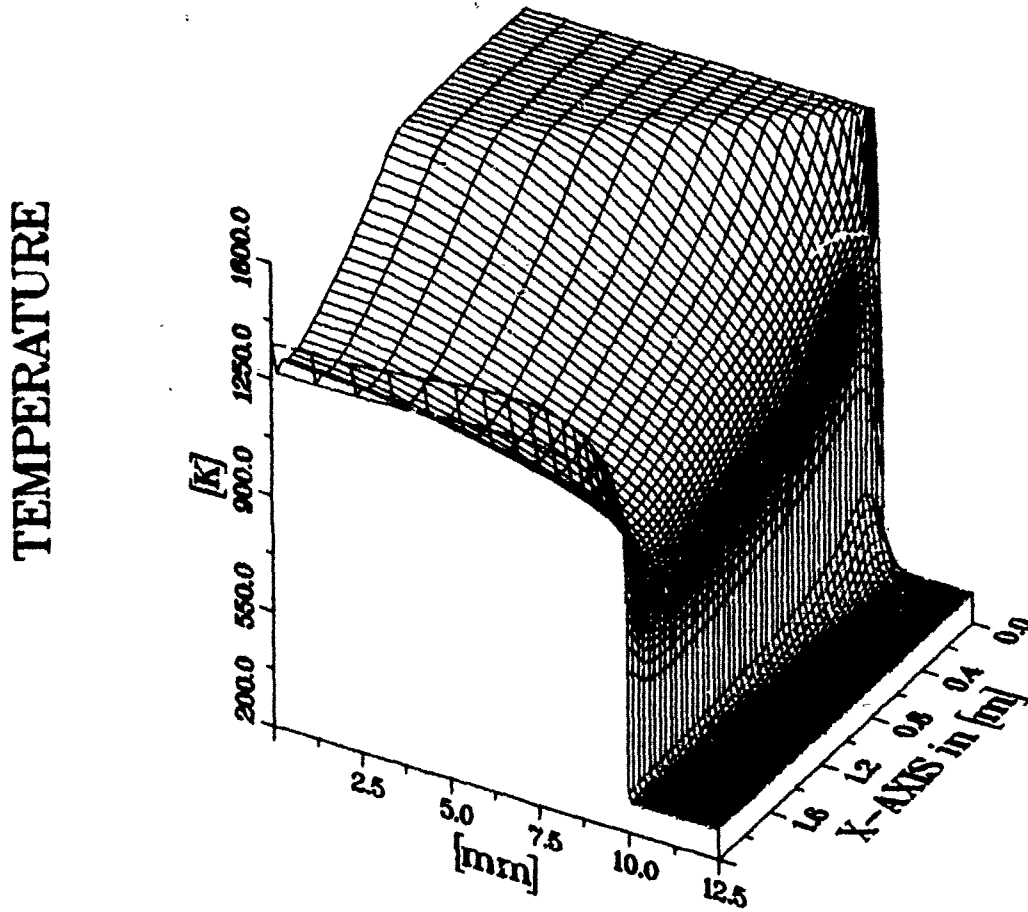


Fig. 12: Spatial temperature distribution in gas and wall

TIME-STEP= 582    TIME= 5.809 [ms]  
PROJ. DISPLACEMENT=2.000 [m]    PROJ. VEL.= 941 [m/s]

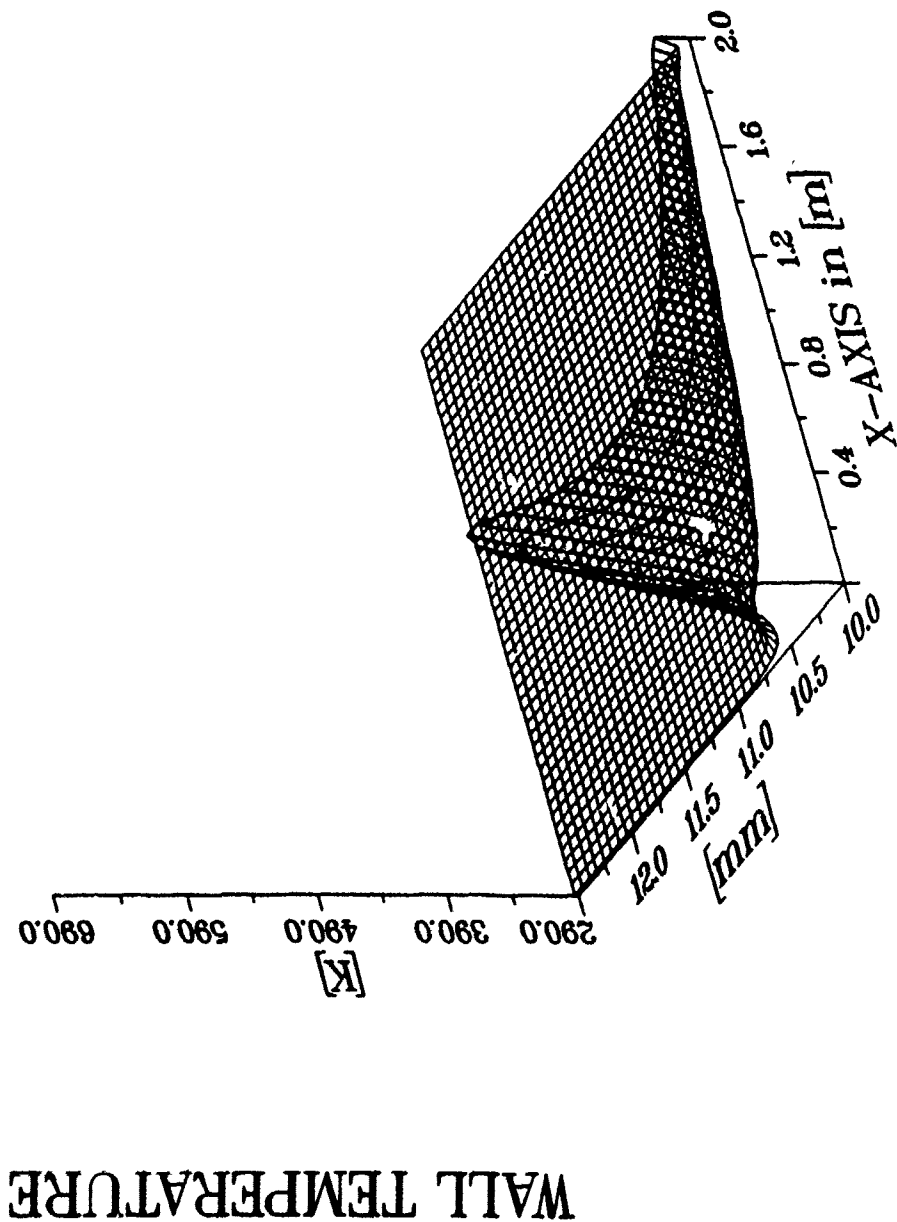


Fig. 13: Wall temperature at muzzle clearance

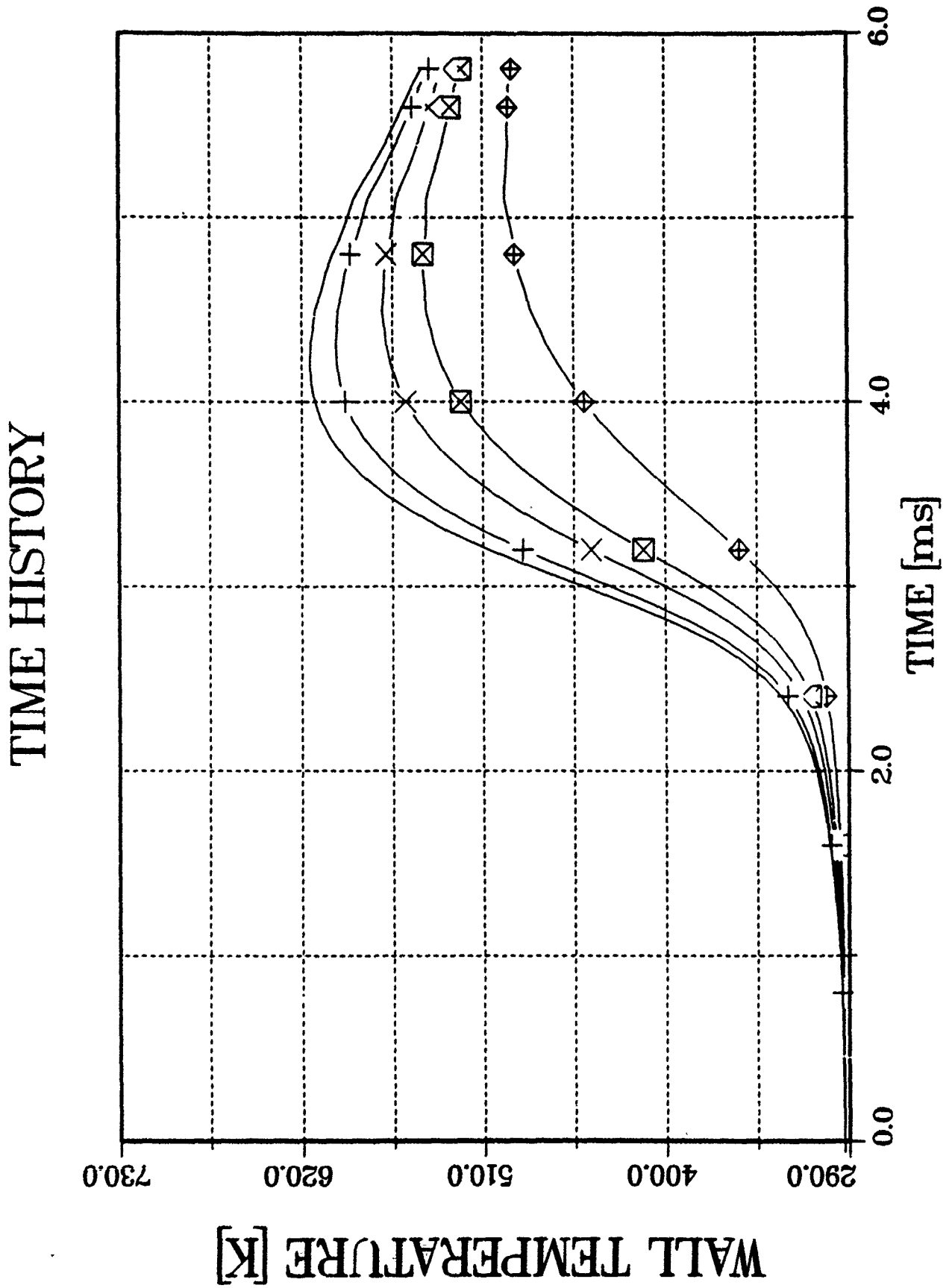


Fig. 14: Temperature in the wall versus time 100 mm off the breach for the surface and the depths 10, 30, 50 and 100  $\mu\text{m}$

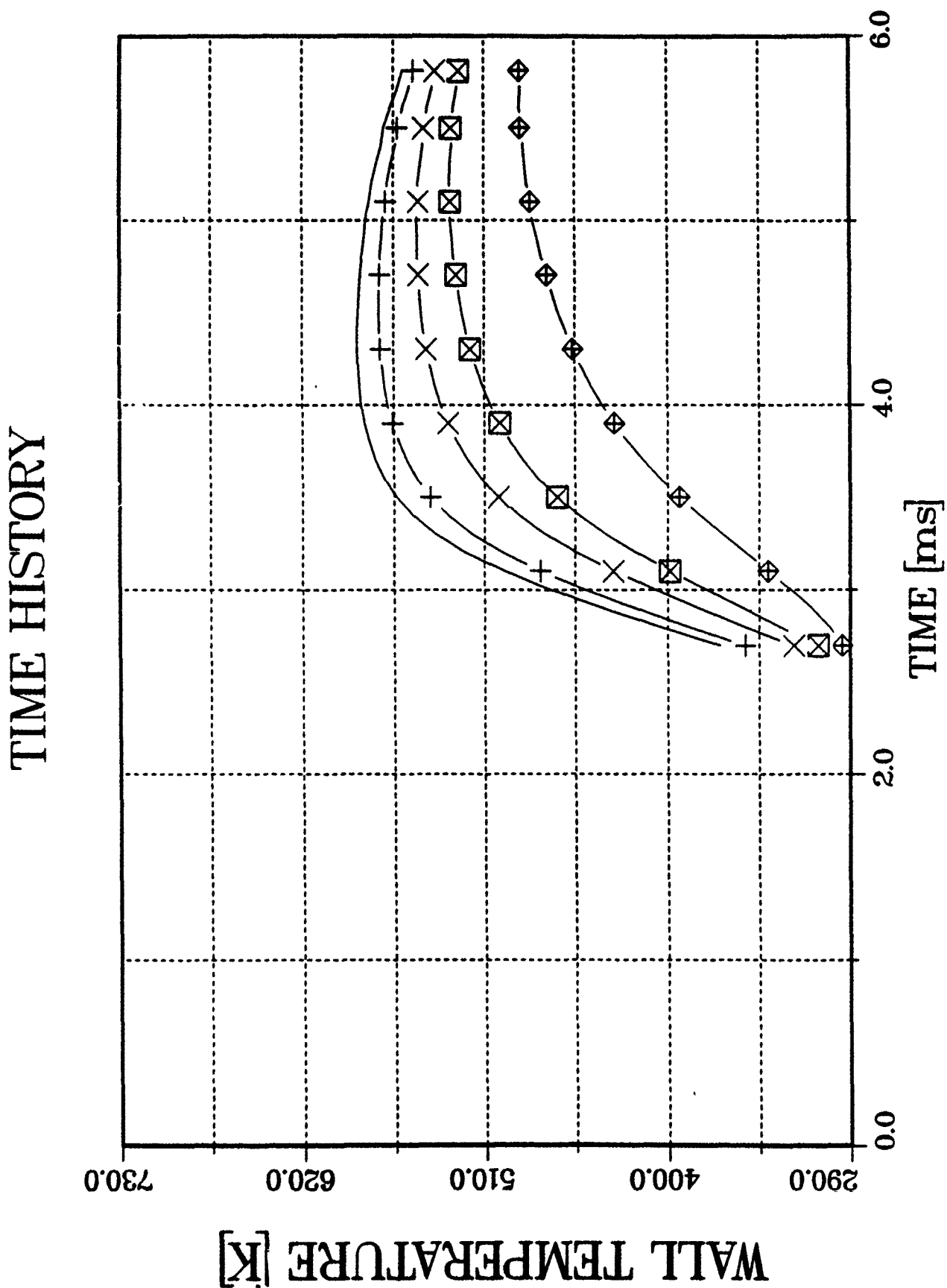


Fig. 15: Temperature in the wall versus time 200 mm off the breach for the surface and the depths 10, 30, 50 and 100 μm

# TIME HISTORY

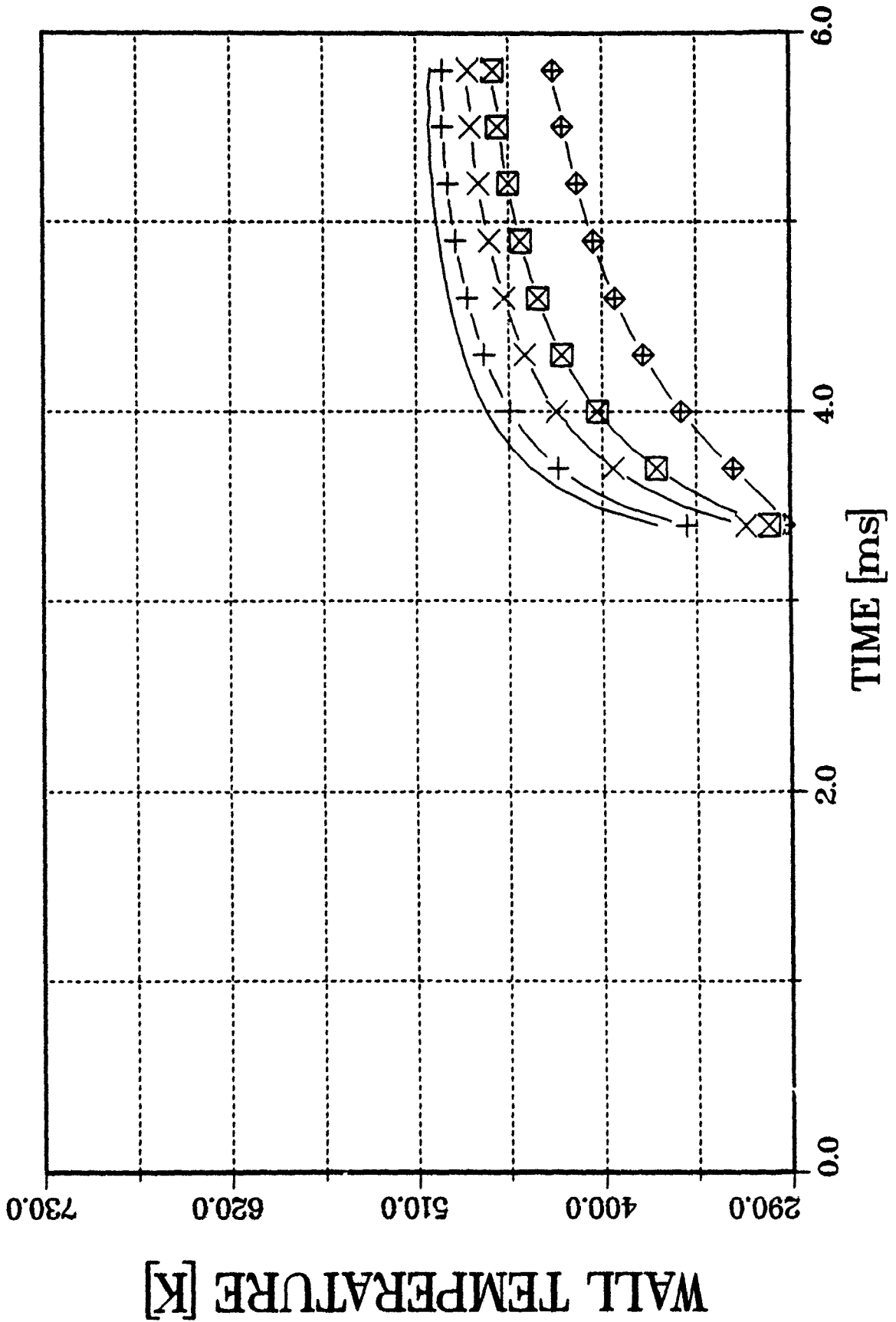


Fig. 16: Temperature in the wall versus time 300 mm off the breach for the surface and the depths 10, 30, 50 and 100 μm

TIME-STEP= 582    TIME= 5.809[ms]  
PROJ. POSITION=2.000[m], PROJ. VEL.= 941.1[m/s]

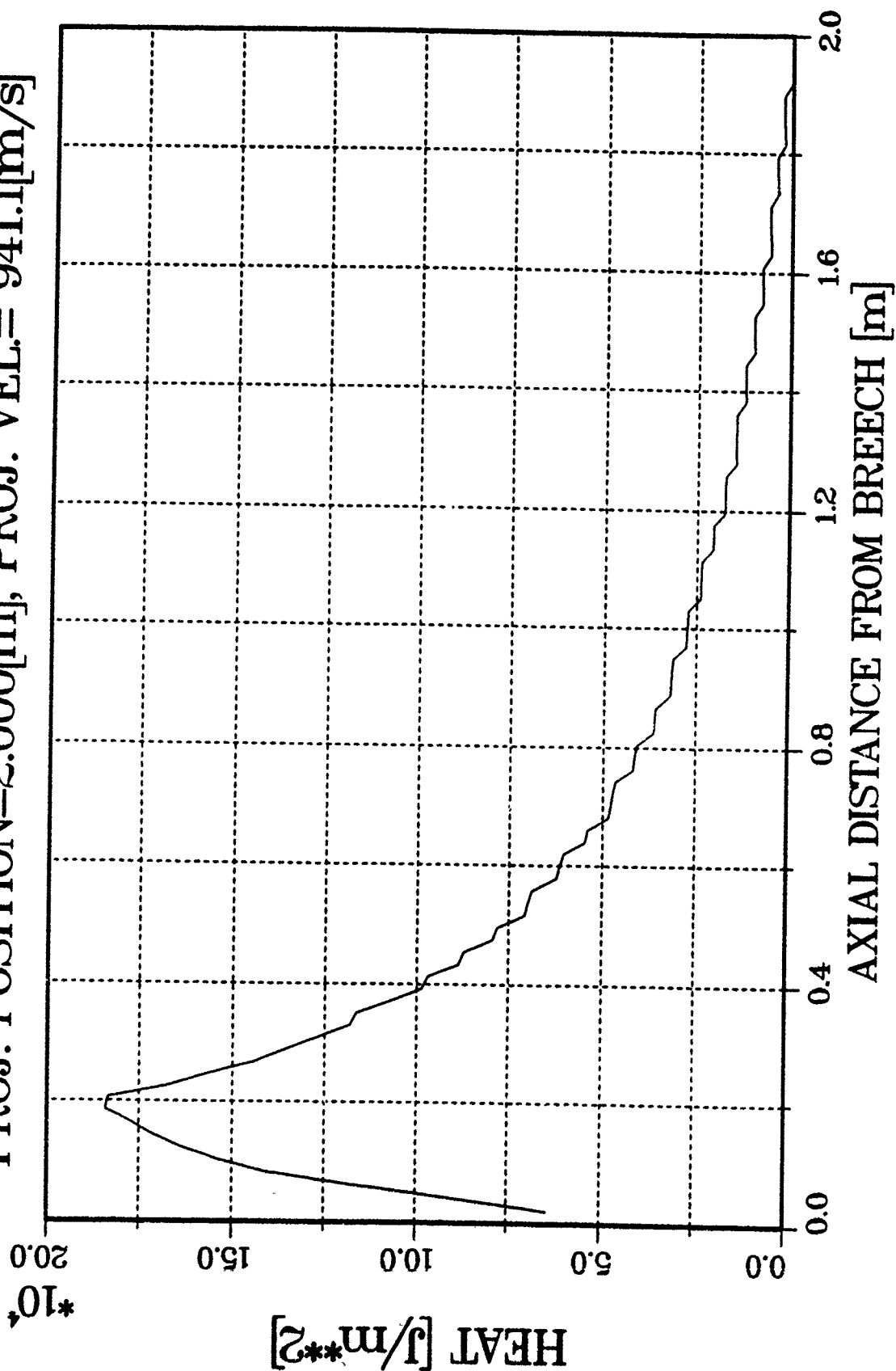


Fig. 17: Amount of heat transfered to the wall

TIME--STEP= 390 TIME= 3.900[ms]  
PROJ. POSITION=0.496[m], PROJ. VEL.= 498.2[m/s]

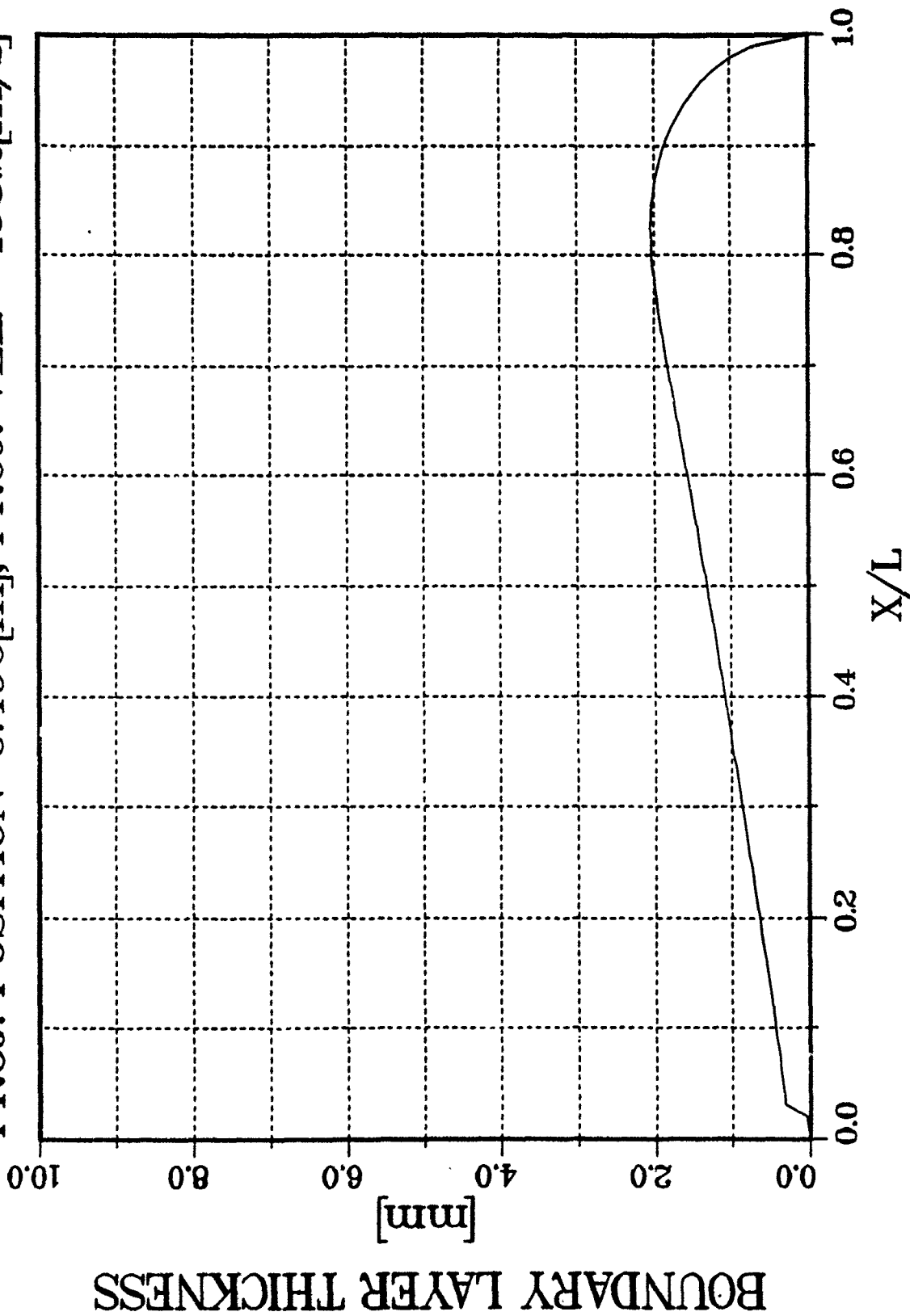


Fig. 18: Velocity boundary layer at 3.9 ms

TIME-STEP= 440 TIME= 4.400[ms]  
PROJ. POSITION=0.800[m], PROJ. VEL.= 704.1[m/s]

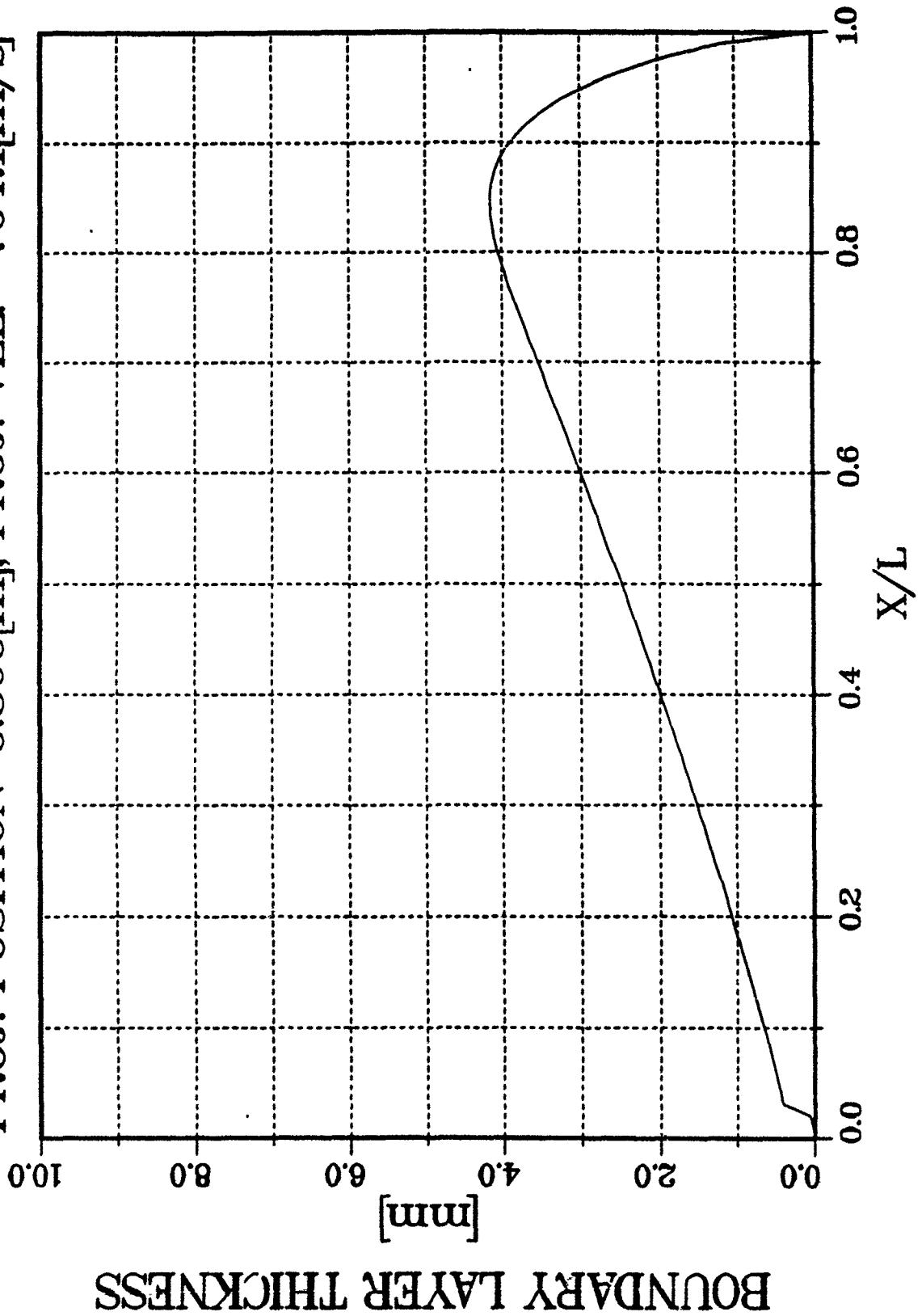


Fig. 19: Velocity boundary layer at 4.4 ms

TIME-STEP= 490 TIME= 4.900[ms]  
PROJ. POSITION=1.187[m], PROJ. VEL.= 830.5[m/s]

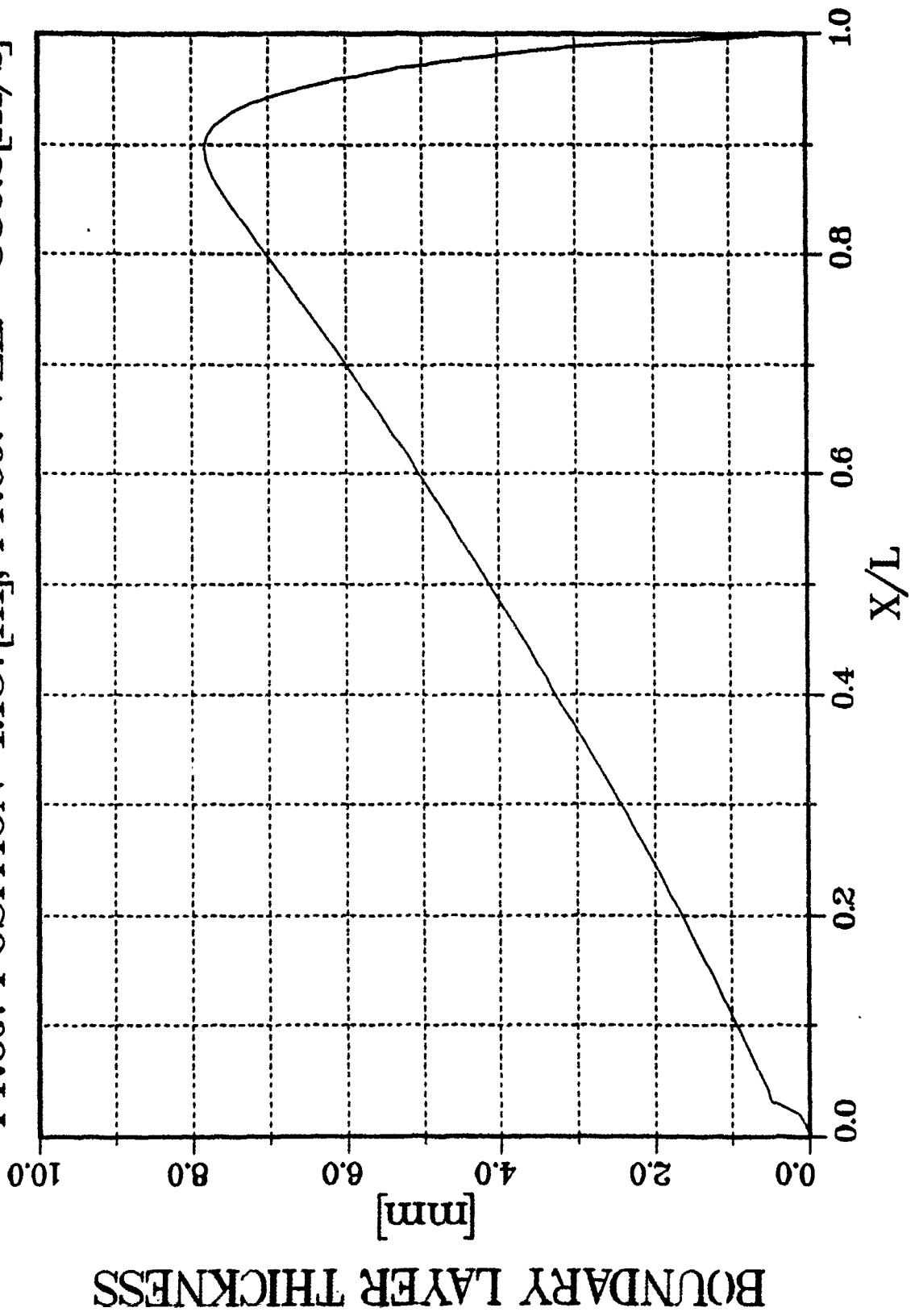


Fig. 20: Velocity boundary layer at 4.9 ms

TIME-STEP= 540 TIME= 5.400[ms]  
PROJ. POSITION=1.622[m], PROJ. VEL.= 903.7[m/s]

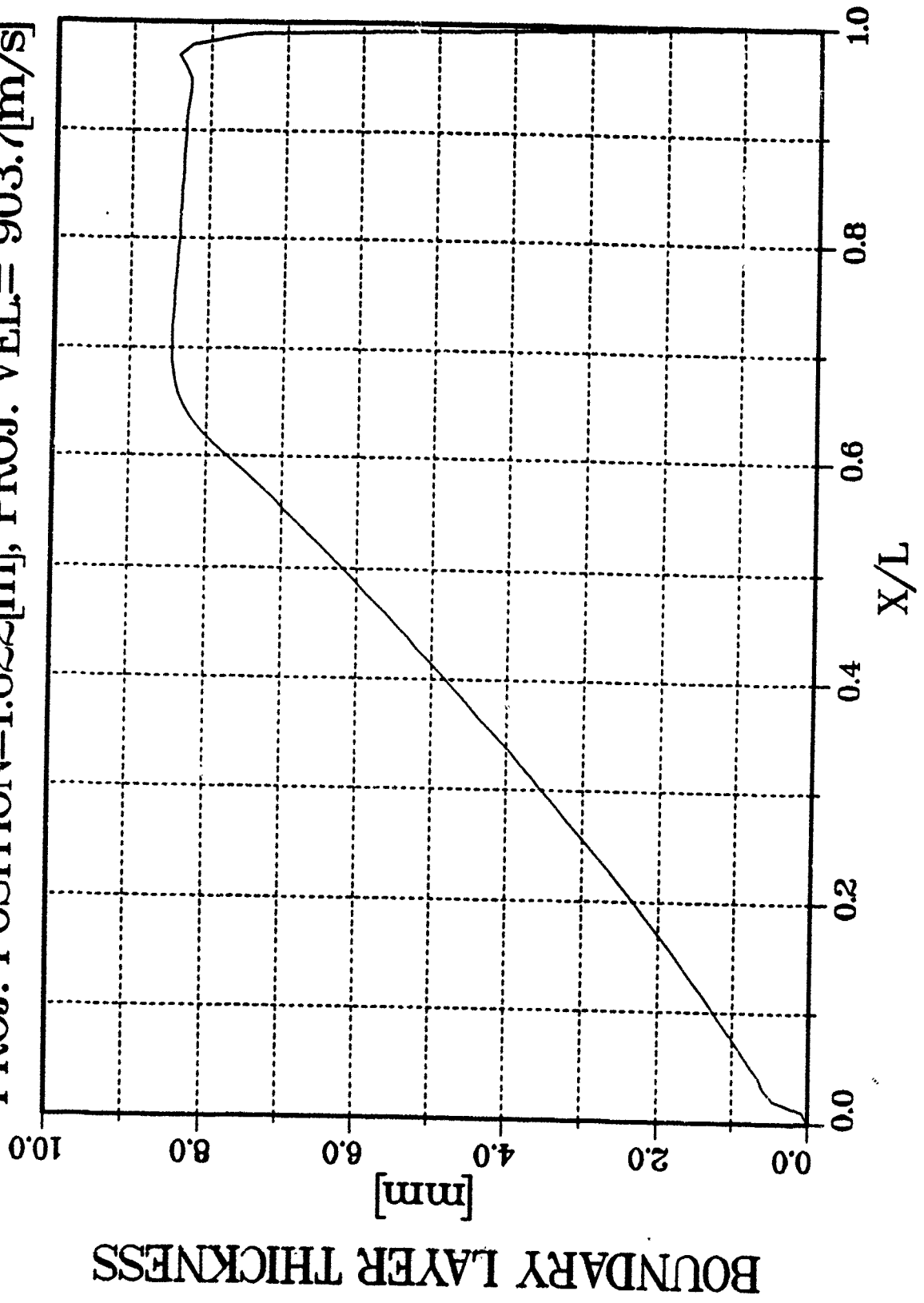


Fig. 21: Velocity boundary layer at 5.4 ms

TIME-STEP= 582    TIME= 5.809[ms]  
PROJ. POSITION=2.000[m], PROJ. VEL.= 941.1[m/s]

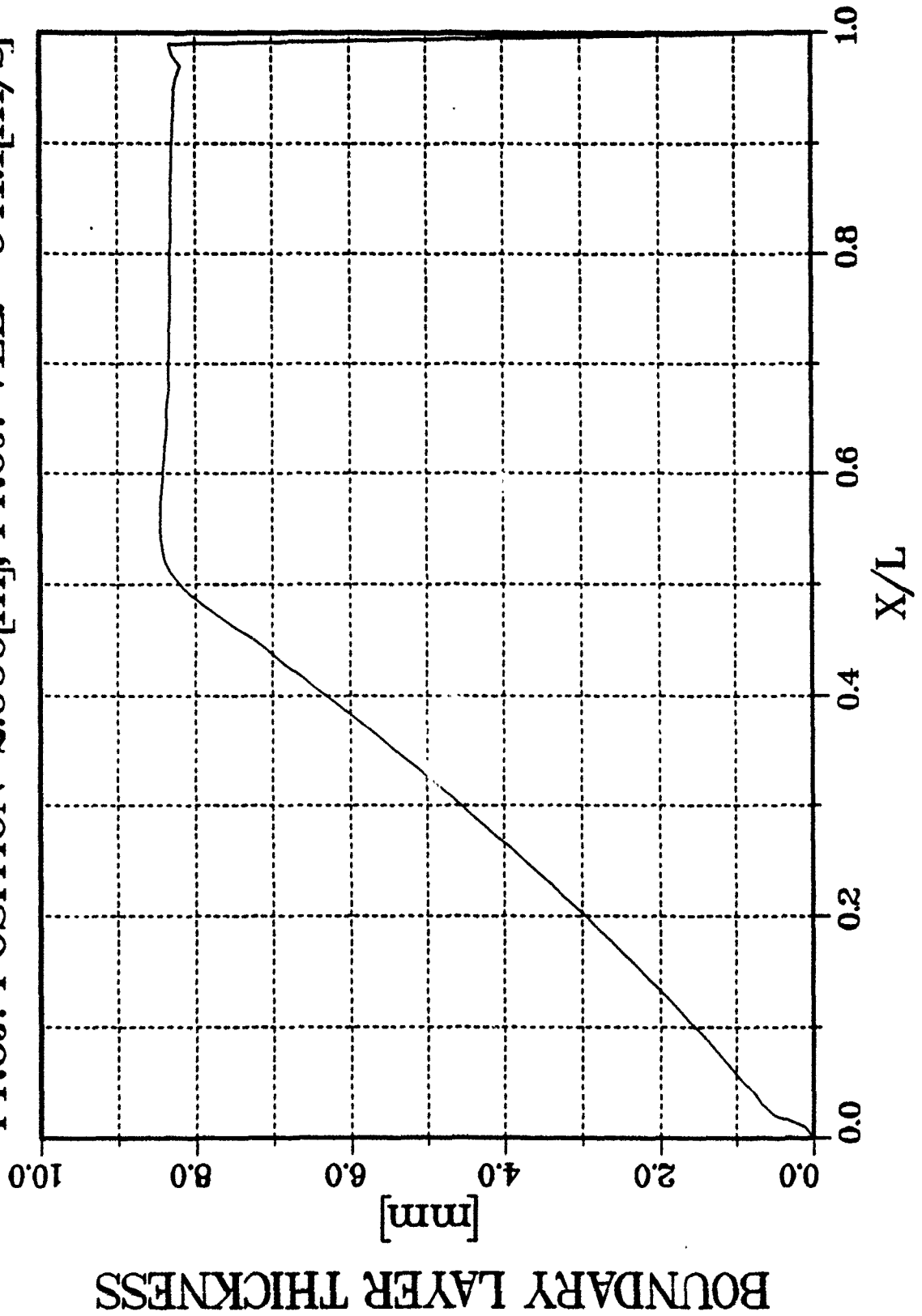


Fig. 22: Velocity boundary layer at muzzle clearance

TIME-STEP= 582 TIME= 5.809[ms]  
PROJ. POSITION=2.000[m], PROJ. VEL.= 941.1[m/s]  
AXIAL DISTANCE FROM BREACH =0.500 [m]

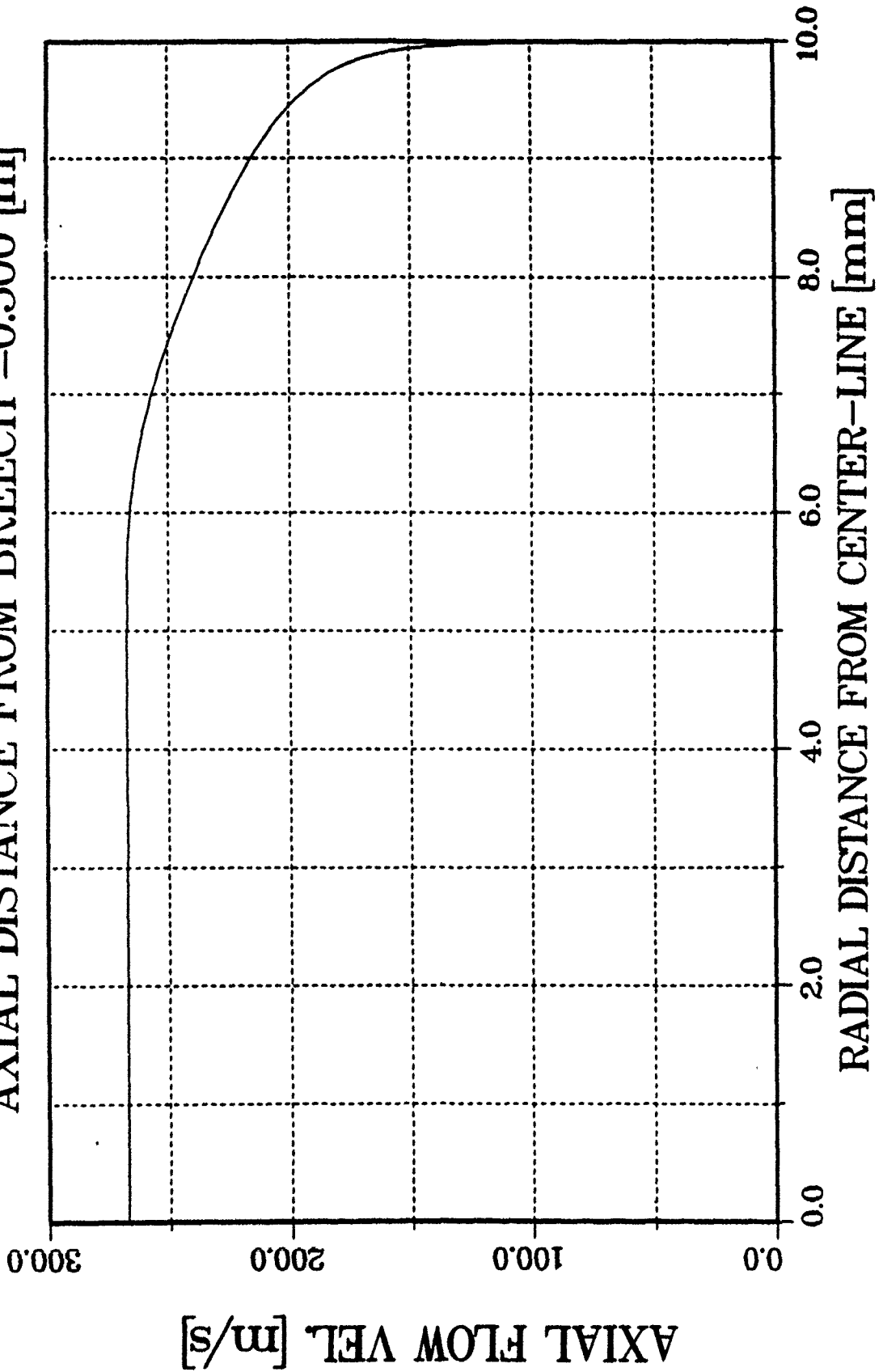


Fig. 23: Radial profile of the axial flow velocity 0.5 m off the breach at muzzle clearance

TIME-STEP= 582    TIME= 5.809[ms]  
PROJ. POSITION=2.000[m], PROJ. VEL.= 941.1[m/s]  
AXIAL DISTANCE FROM BREACH =1.500 [m]

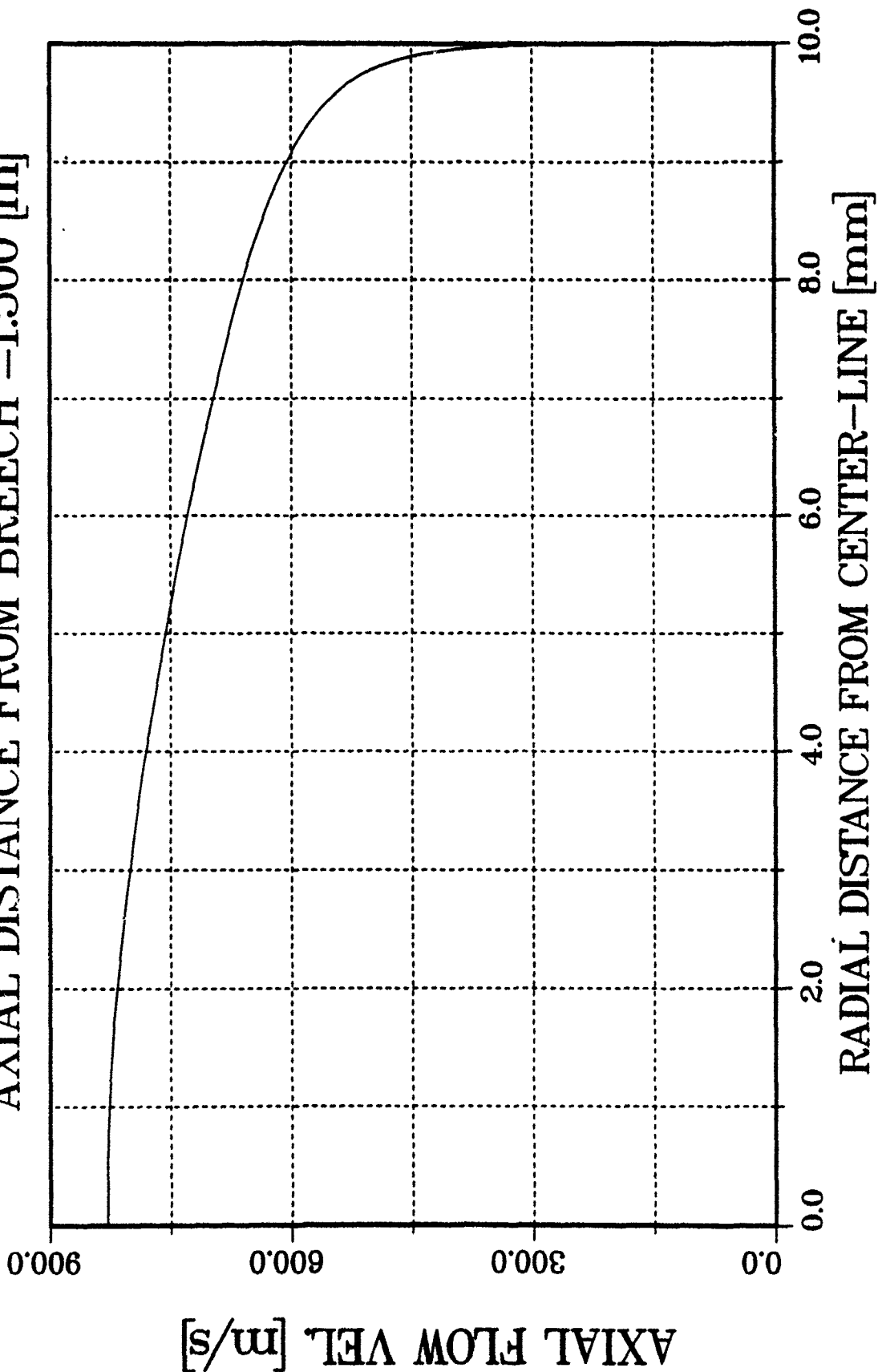


Fig. 24: Radial profile of the axial flow velocity 1.5 m off the breach at muzzle clearance

TIME-STEP= 582    TIME= 5.809[ms]  
PROJ. POSITION=2.000[m], PROJ. VEL.= 941.1[m/s]  
AXIAL DISTANCE FROM BREECH =1.950 [m]

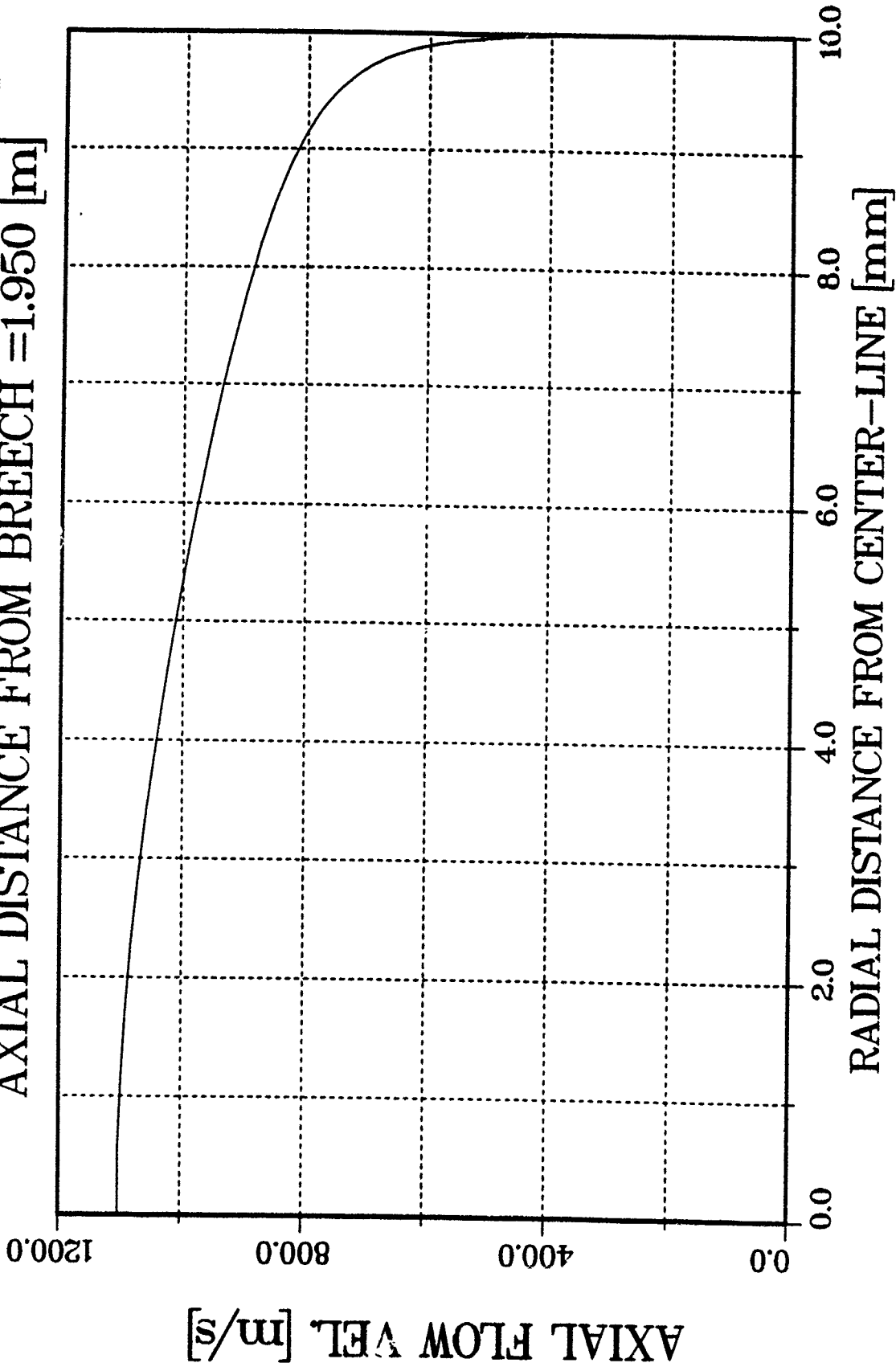


Fig. 25: Radial profile of the axial flow velocity 1.95 m off the breech at muzzle clearance

Small vertical text on the right edge of the page, likely a page number or document identifier.

TIME-STEP= 582    TIME= 5.809[ms]  
PROJ. POSITION=2.000[m], PROJ. VEL.= 941.1[m/s]  
AXIAL DISTANCE FROM BREACH =0.500 [m]

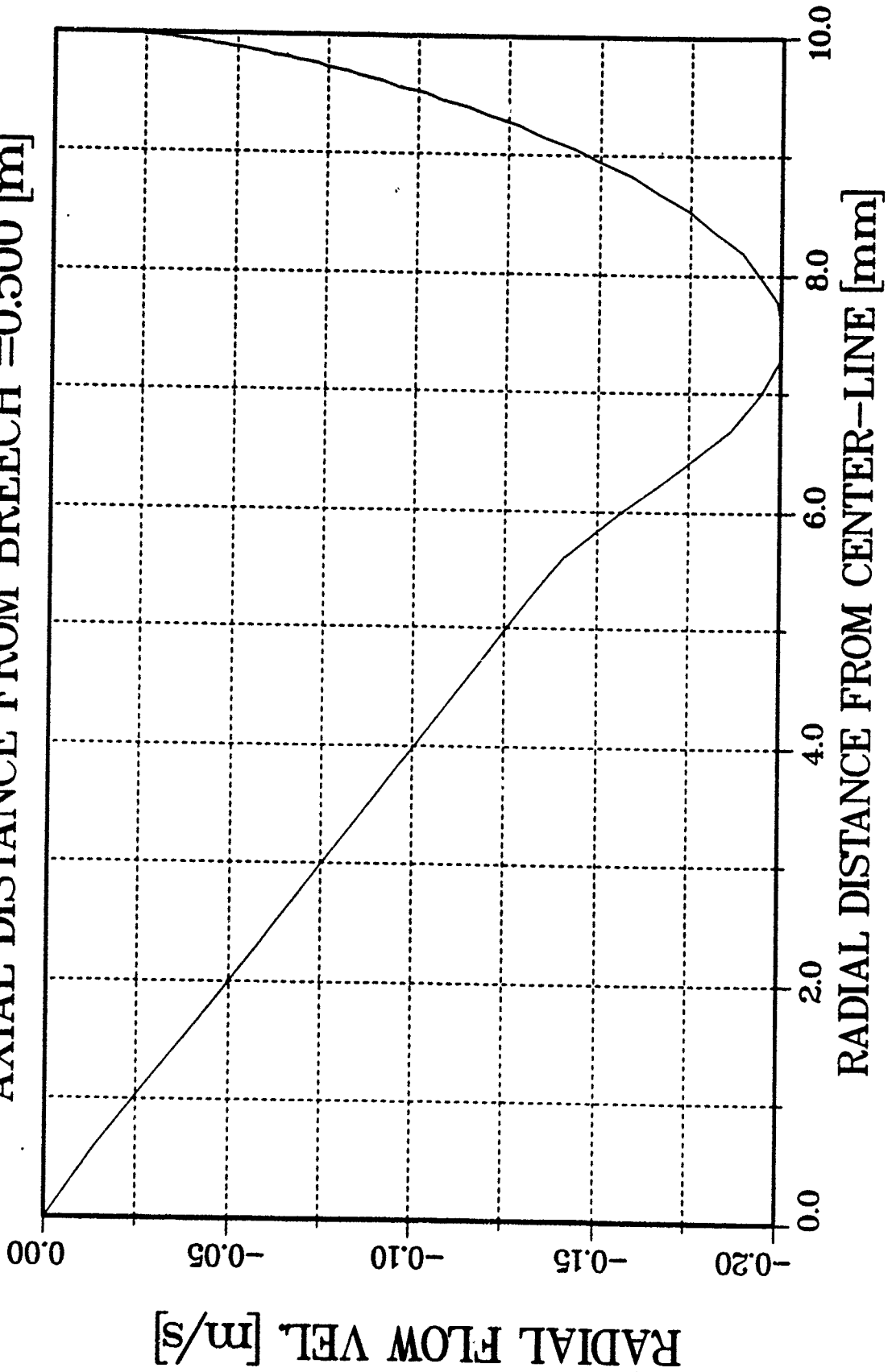


Fig. 26: Radial profile of the radial flow velocity 0.5 m off the breach at muzzle clearance

TIME-STEP= 582    TIME= 5.809[ms]  
PROJ. POSITION=2.000[m], PROJ. VEL.= 941.1[m/s]  
AXIAL DISTANCE FROM BREACH =1.500 [m]

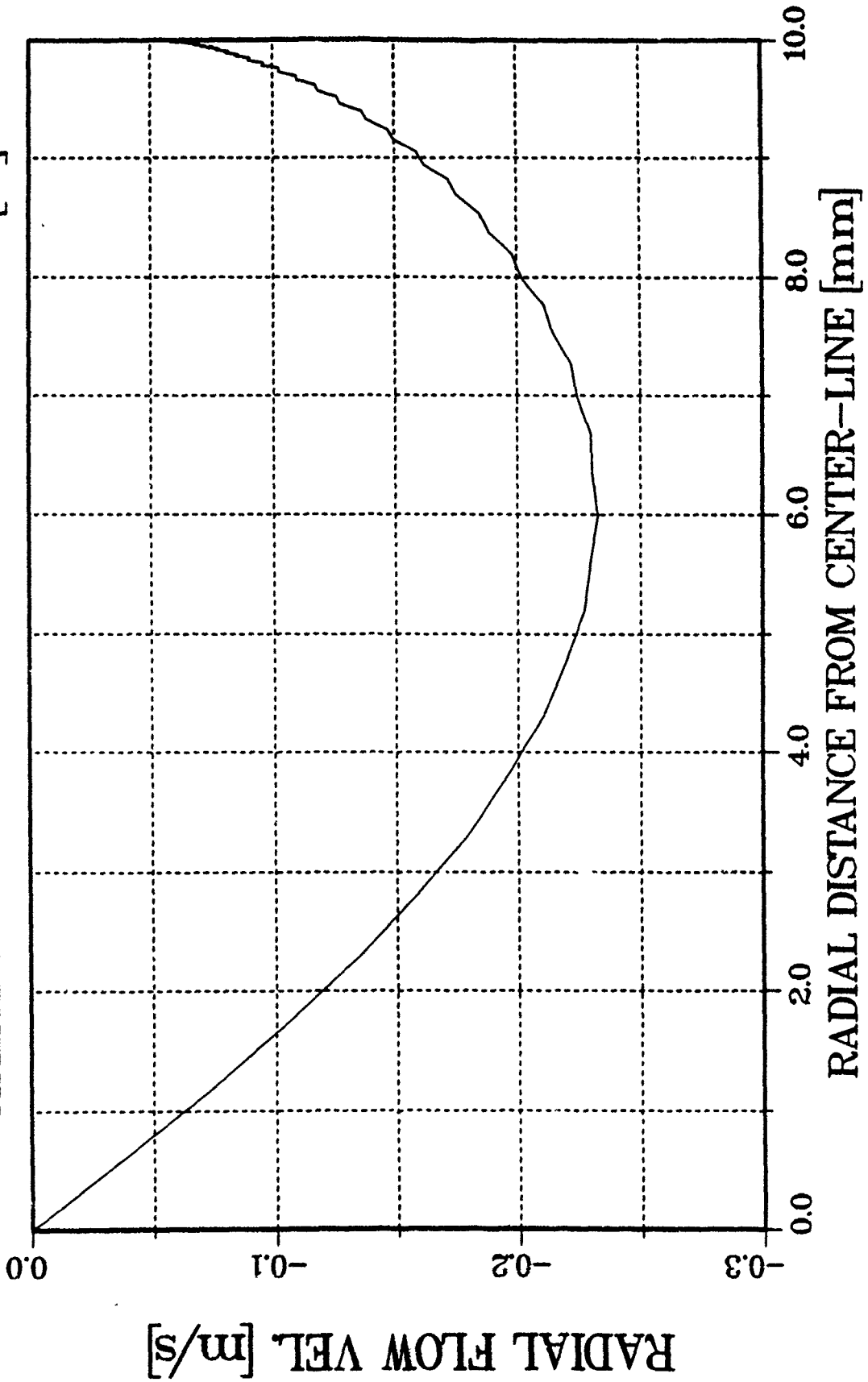


Fig. 27: Radial profile of the radial flow velocity 1.5 m off the breach at muzzle clearance

TIME-STEP= 582 TIME= 5.809[ms]  
PROJ. POSITION=2.000[m], PROJ. VEL.= 941.1[m/s]  
AXIAL DISTANCE FROM BREACH =1.950 [m]

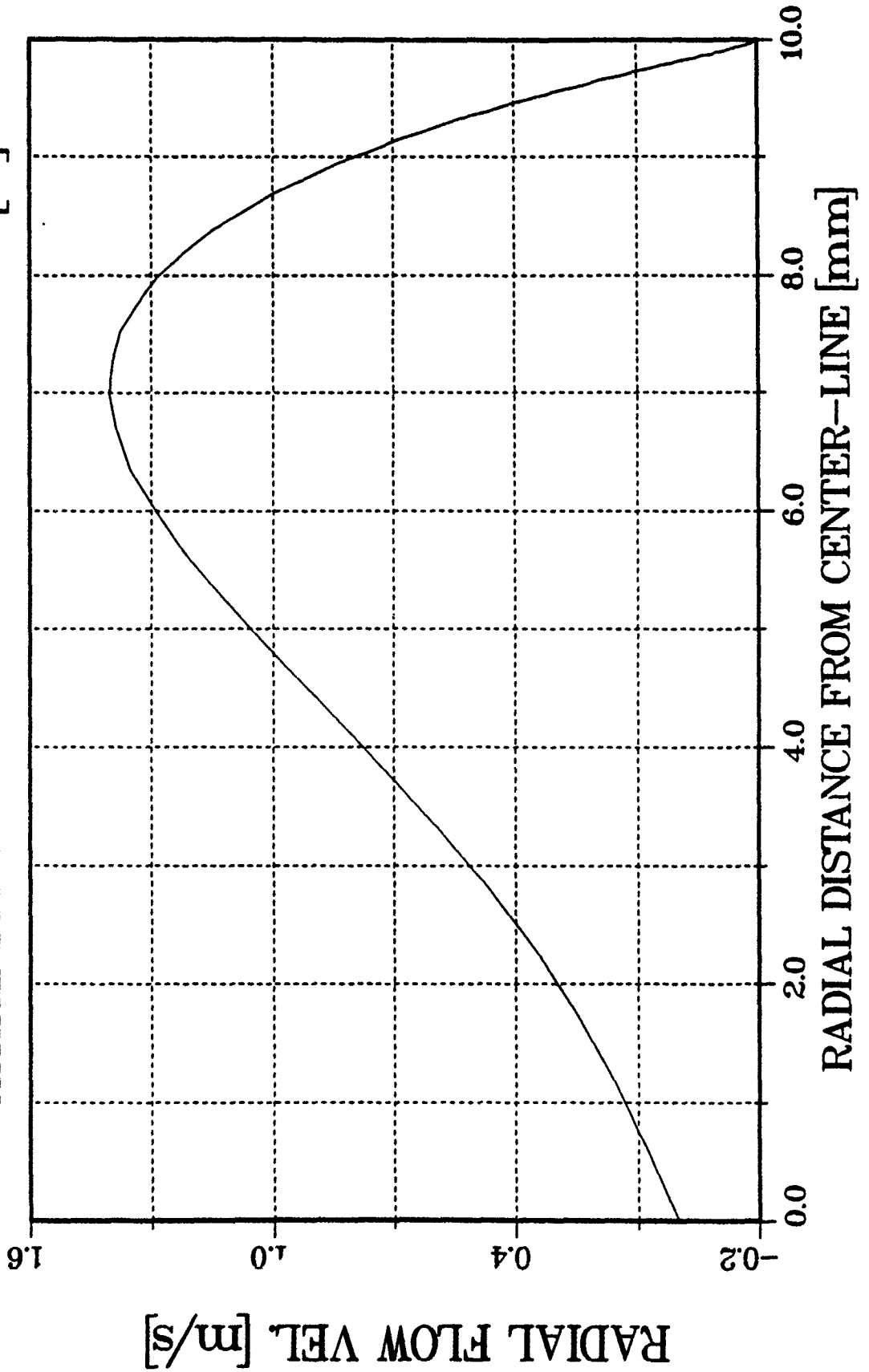


Fig. 28: Radial profile of the radial flow velocity 1.95 m off the breach at muzzle clearance

TIME-STEP= 582    TIME= 5.809[ms]  
PROJ. POSITION=2.000[m], PROJ. VEL.= 941.1[m/s]  
AXIAL DISTANCE FROM BREACH =0.500 [m]

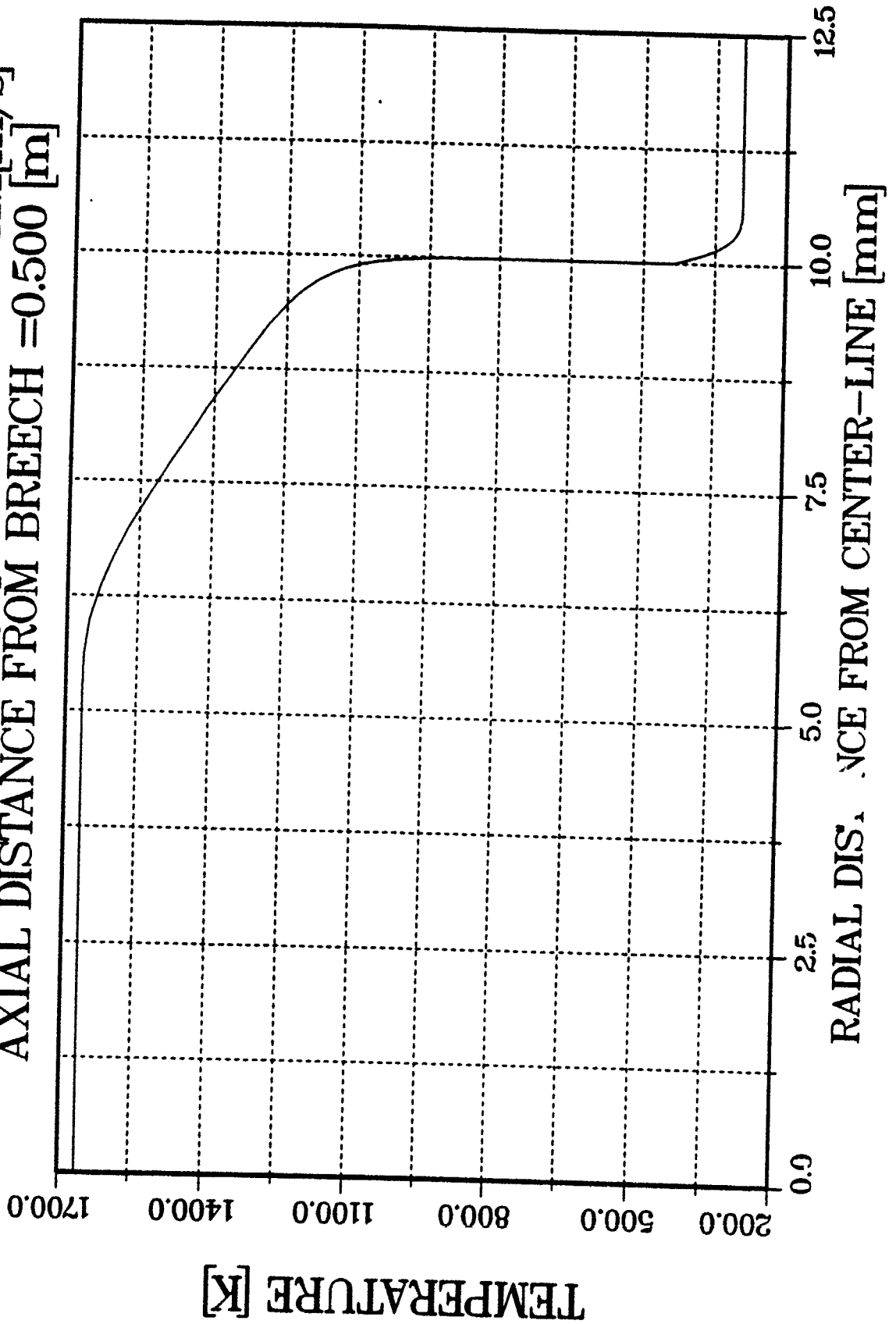


Fig. 29: Radial profile of the temperature in gas and wall 0.5 m off the breach at muzzle clearance

TIME-STEP= 582    TIME= 5.809[ms]  
PROJ. POSITION=2.000[m], PROJ. VEL.= 941.1[m/s]  
AXIAL DISTANCE FROM BREACH =1.500 [m]

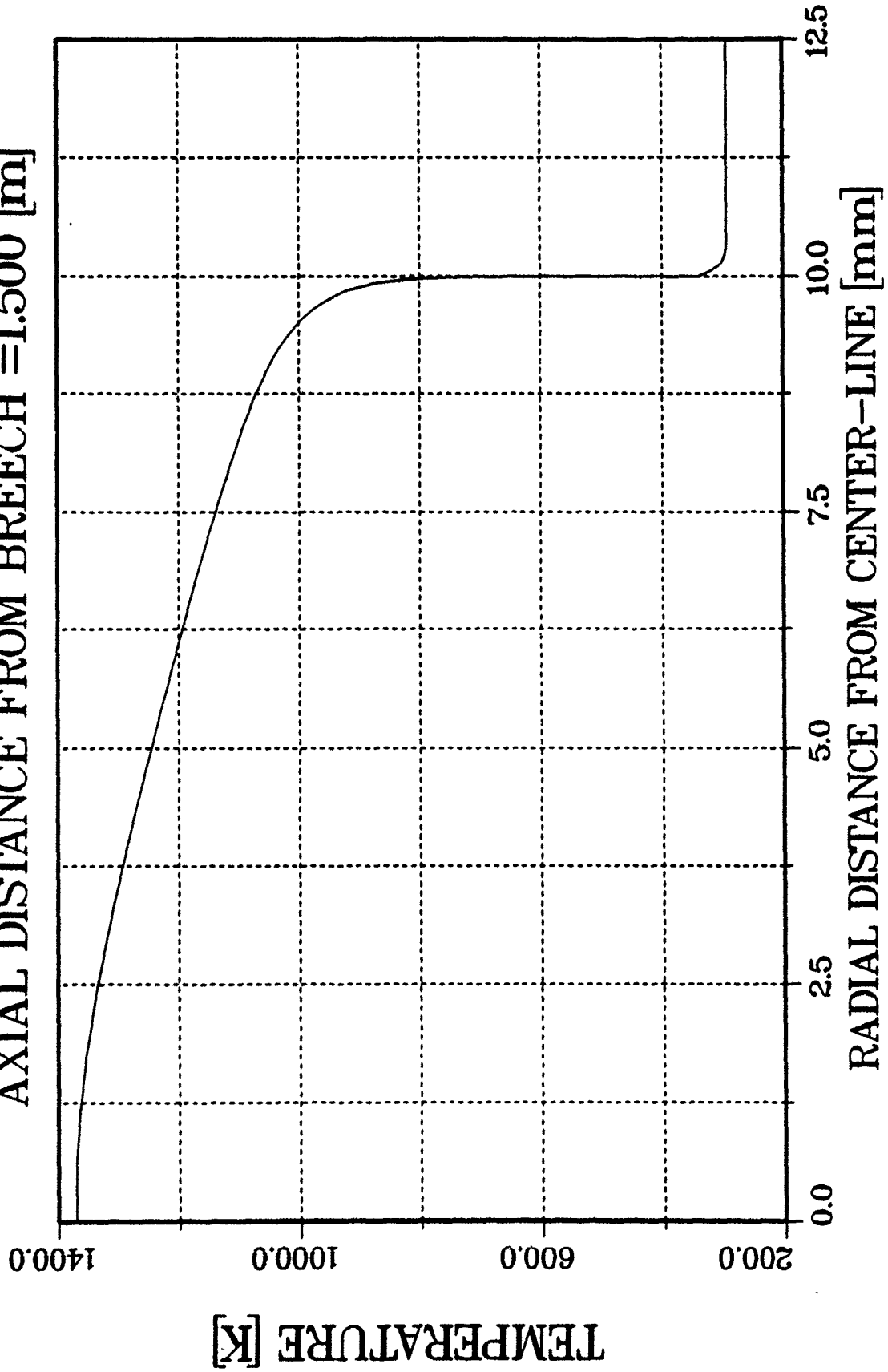


Fig. 30: Radial profile of the temperature in gas and wall 1.5 m off the breach at muzzle clearance

TIME-STEP= 582    TIME= 5.809[ms]  
PROJ. POSITION=2.000[m], PROJ. VEL.= 941.1[m/s]  
AXIAL DISTANCE FROM BREECH =1.950 [m]

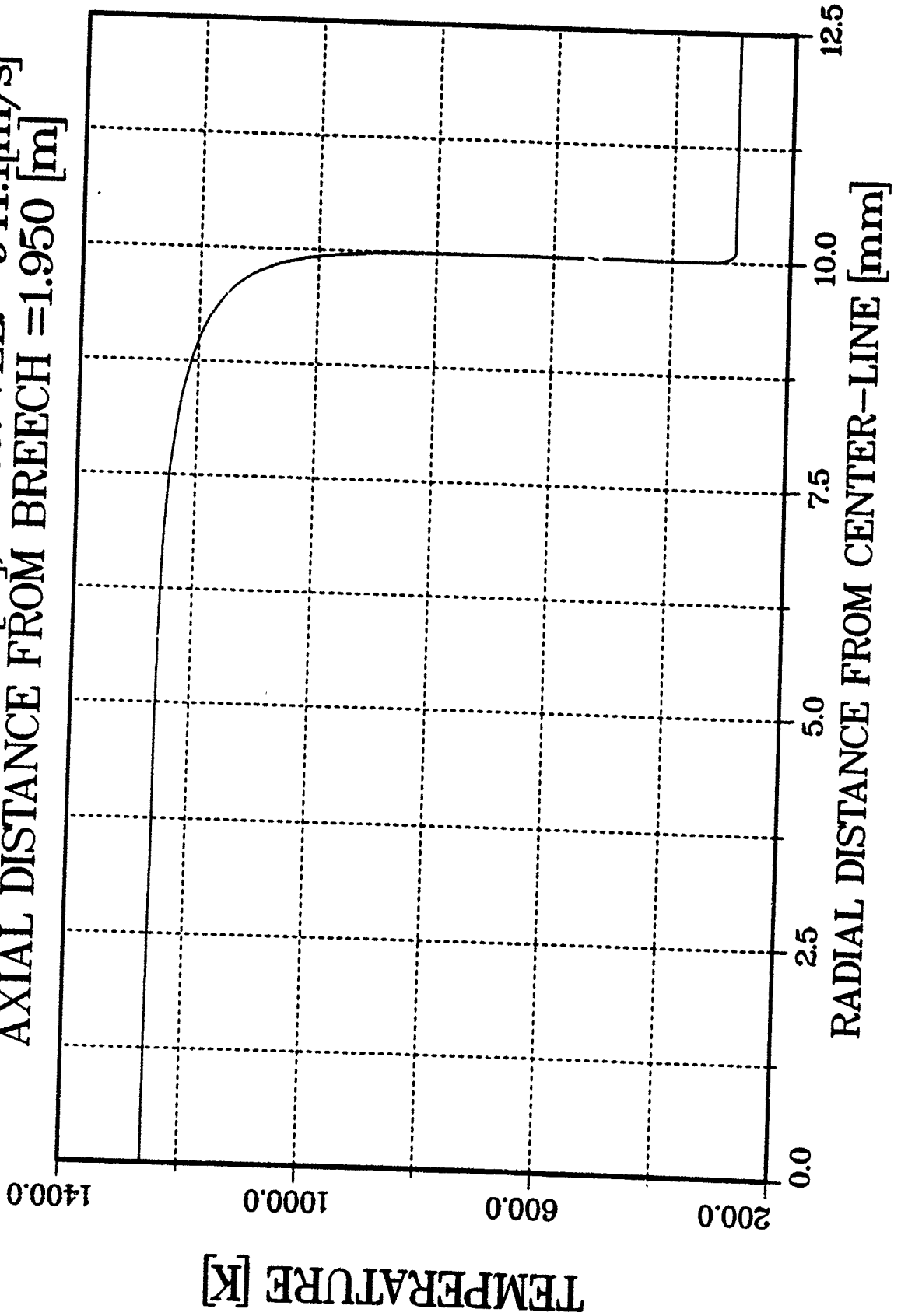


Fig. 31: Radial profile of the temperature in gas and wall 1.95 m off the breech at muzzle clearance

TIME HISTORY

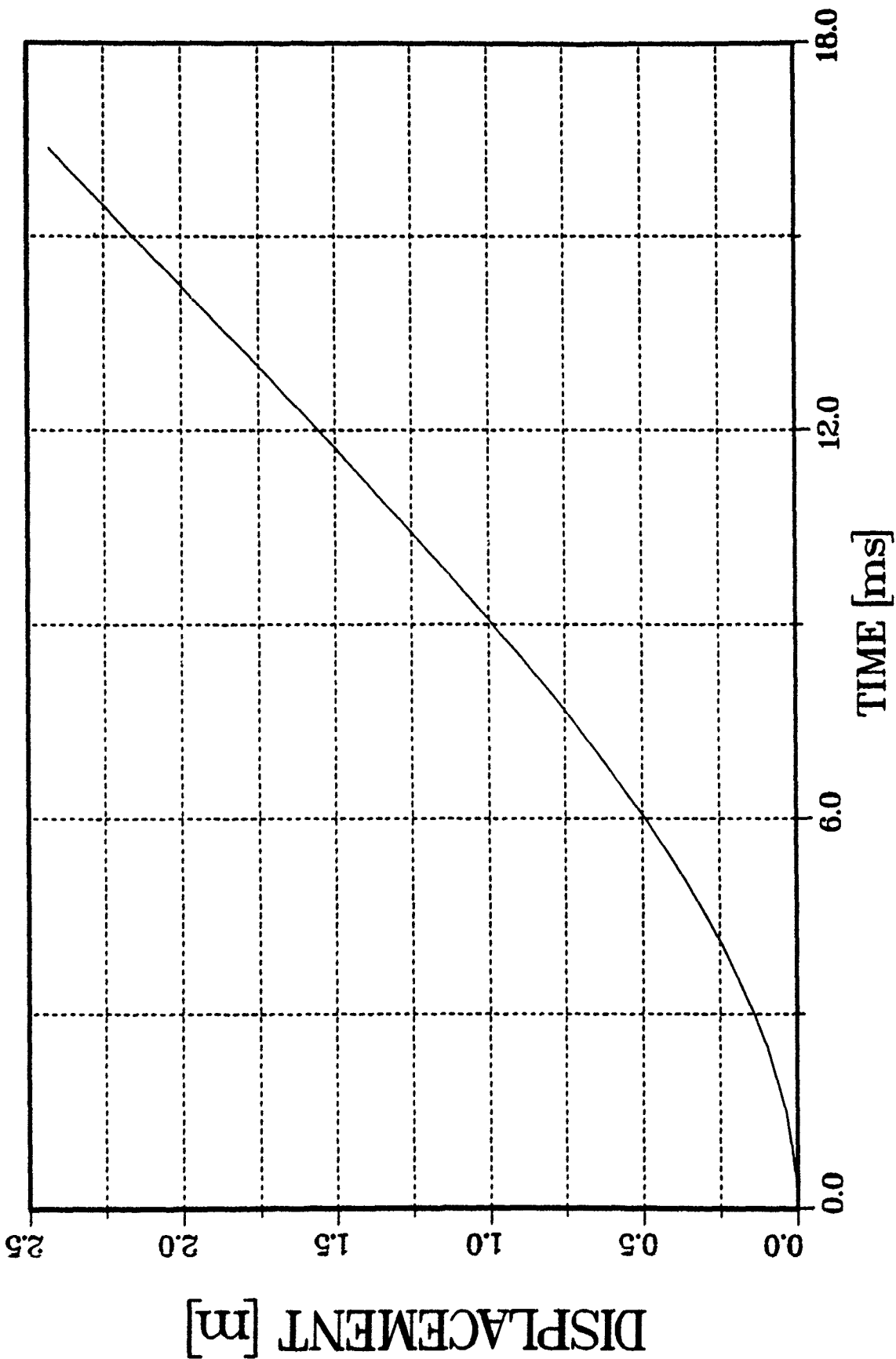


Fig. 32: Projectile displacement versus time

TIME HISTORY

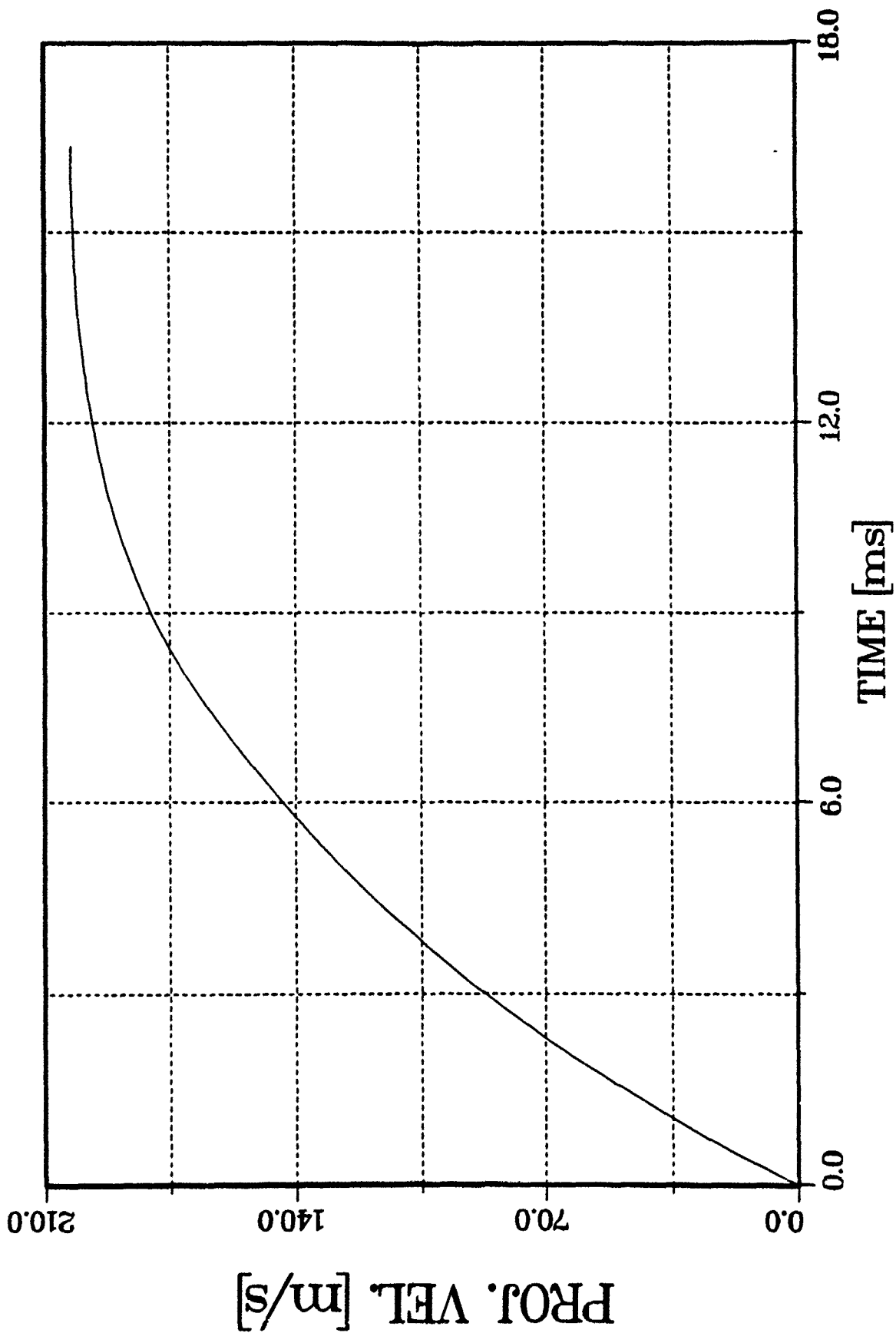


Fig. 33: Projectile velocity versus time

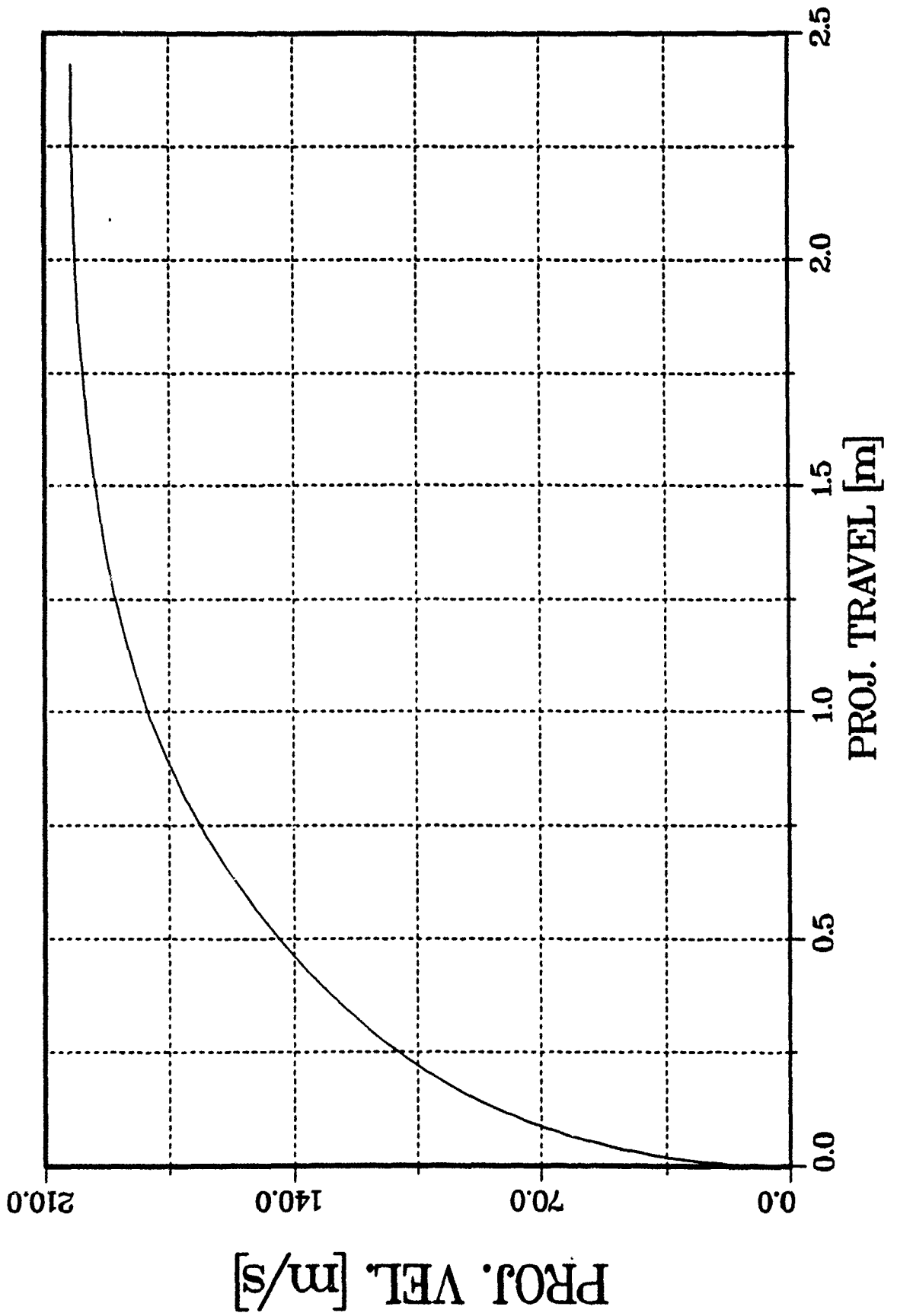


Fig. 34: Projectile velocity versus projectile travel

# TIME HISTORY

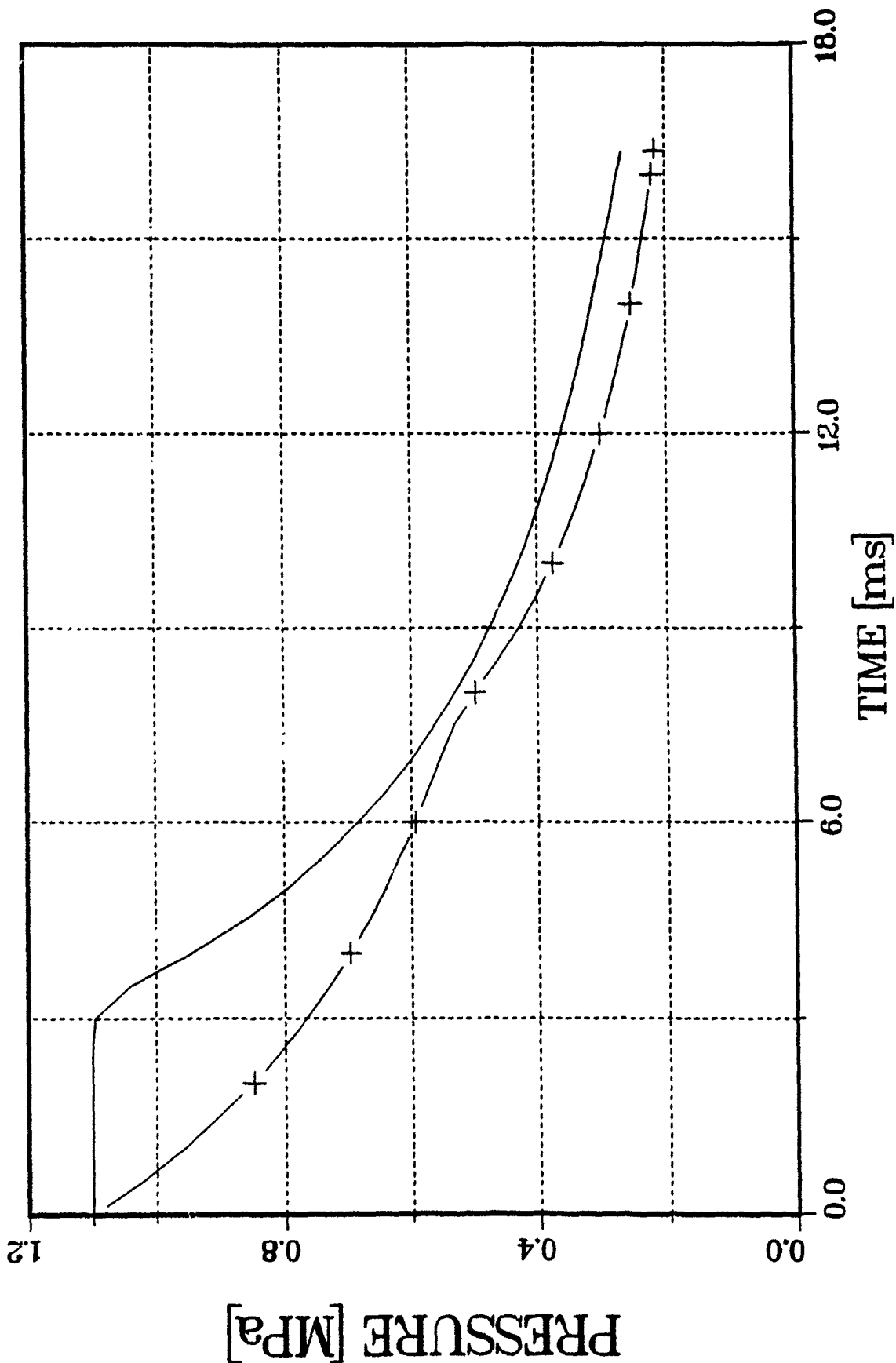


Fig. 35: Gas pressure at the breech and projectile base versus time

TIME HISTORY

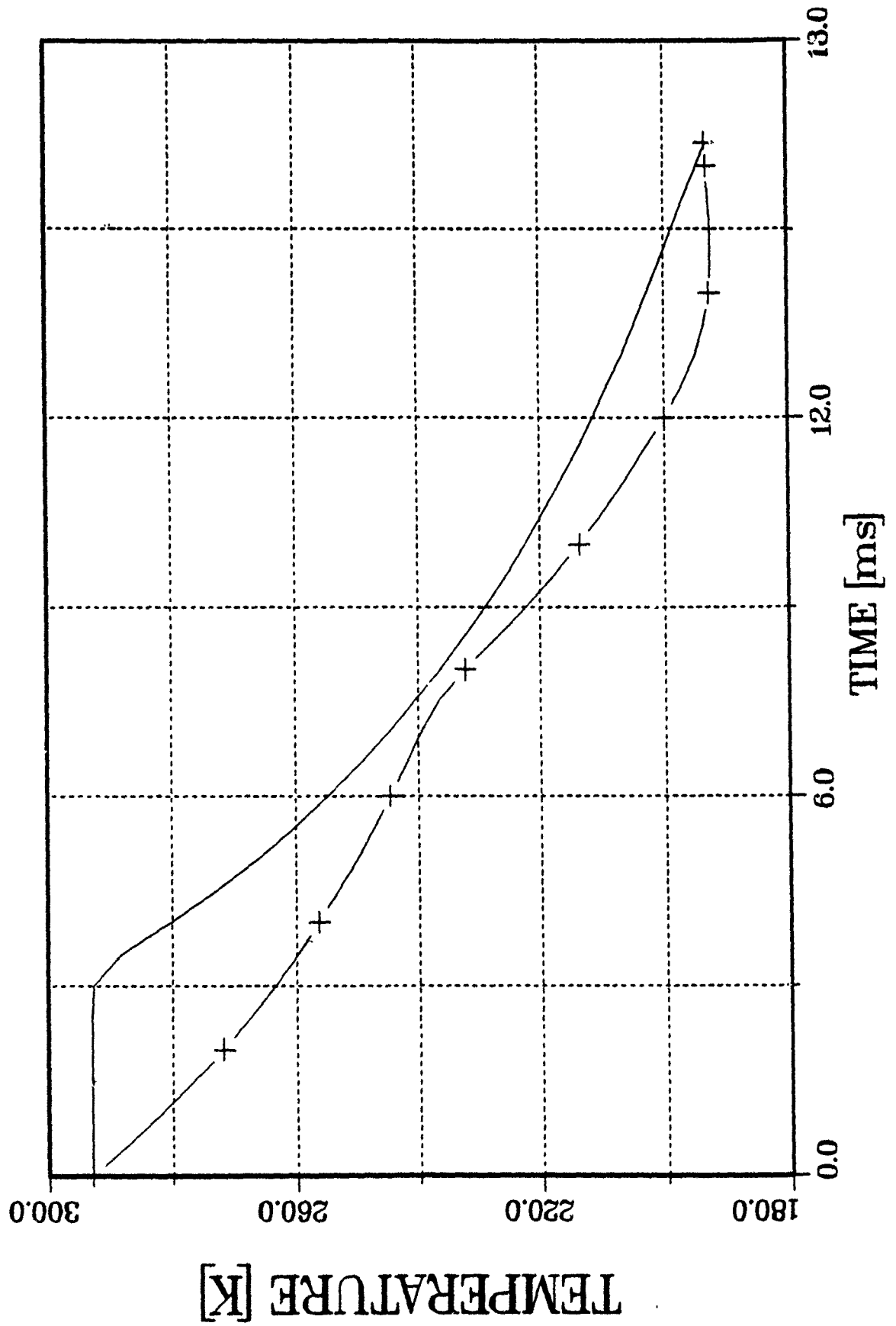


Fig. 36: Gas temperature at the breech and projectile base versus time

TIME HISTORY

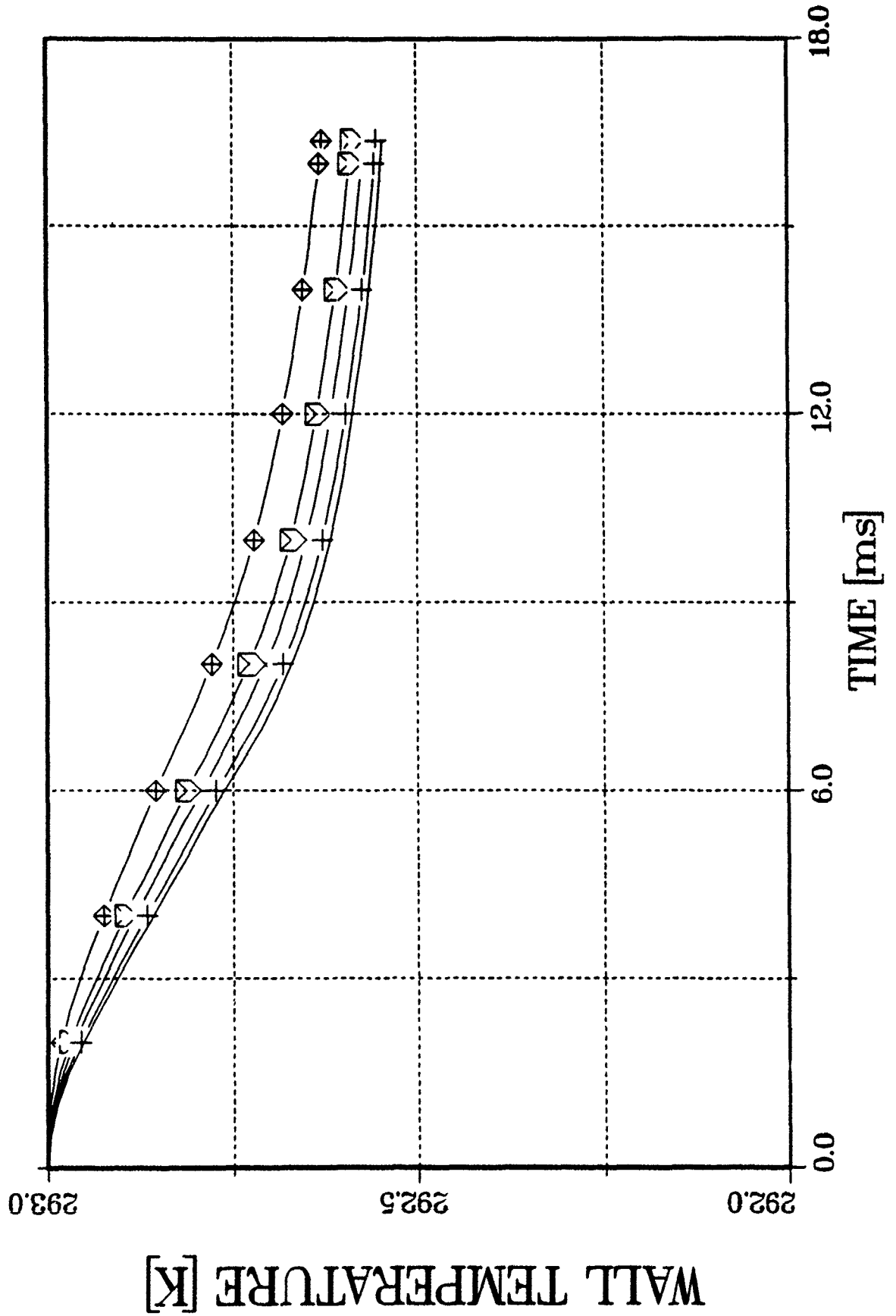


Fig. 37: Temperature in the wall versus time 1.0 m off the breach for the surface and the depths 10, 30, 50 and 100 μm

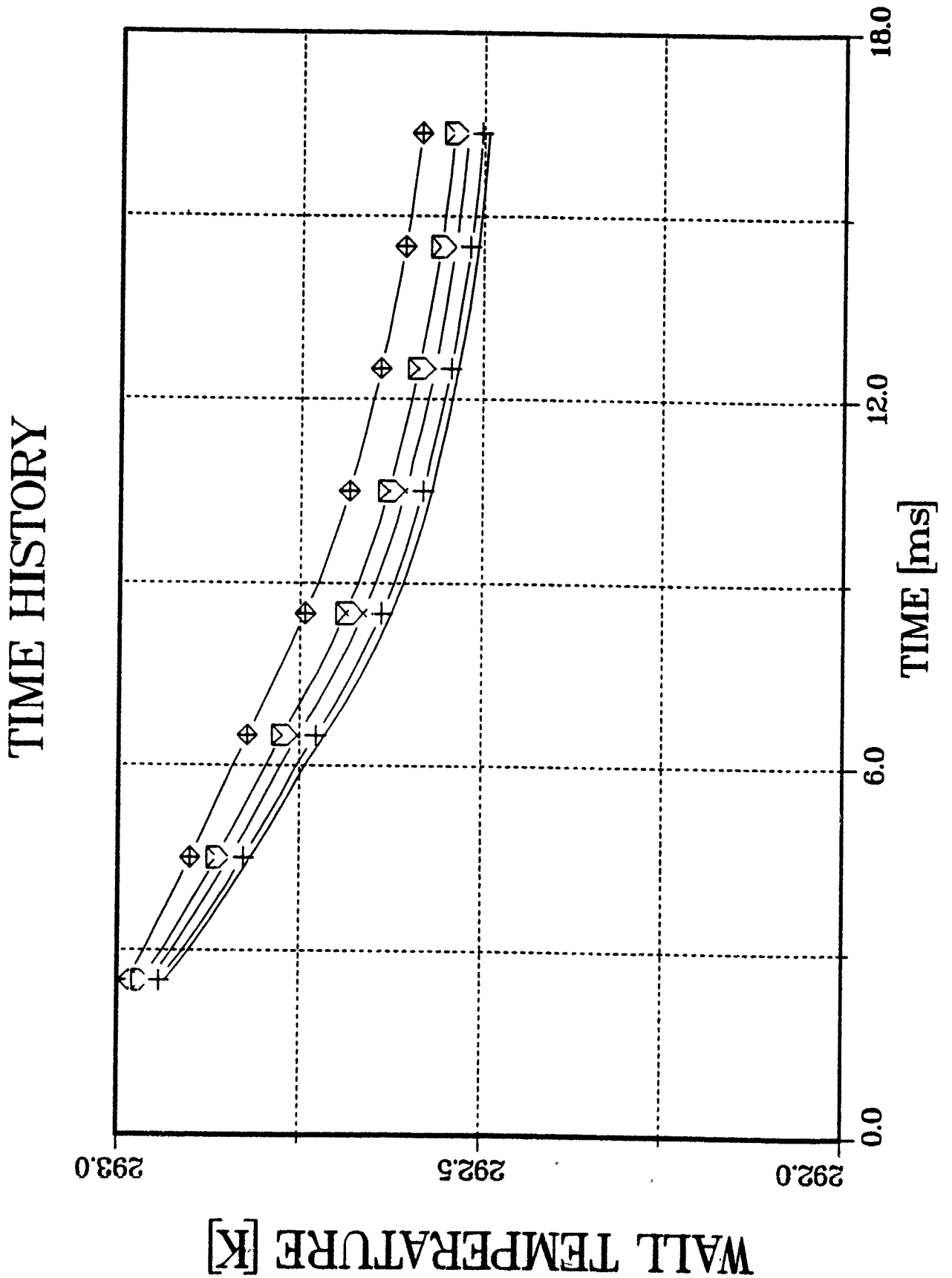


Fig. 38: Temperature in the wall versus time 1.2 m off the breach for the surface and the depths 10, 30, 50 and 100  $\mu\text{m}$

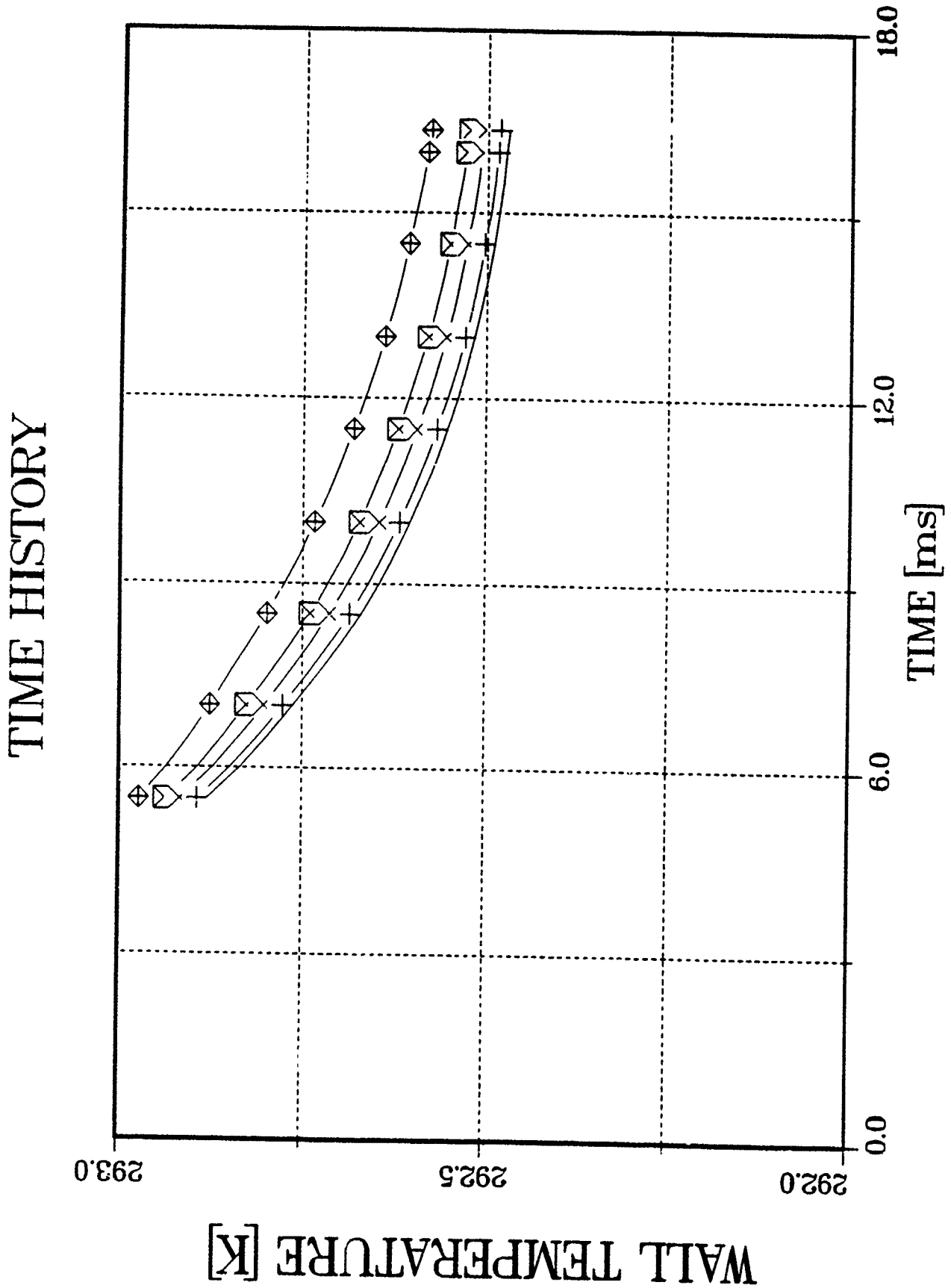


Fig. 39: Temperature in the wall versus time 1.5 m off the breach for the surface and the depths 10, 30, 50 and 100 μm

Vertical text on the right edge of the page, likely a page number or reference code, oriented vertically.

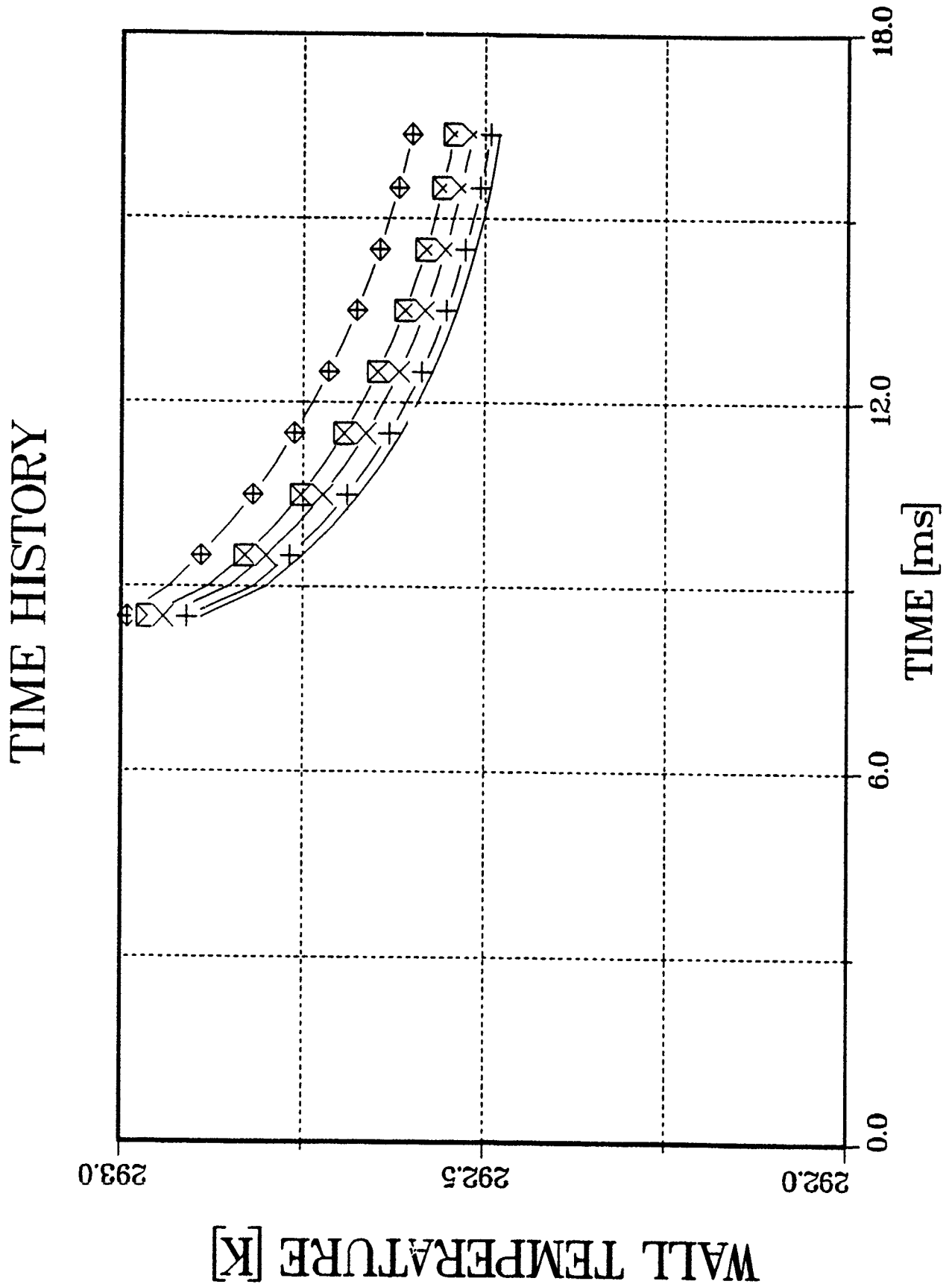


Fig. 40: Temperature in the wall versus time 2.0 m off the breach for the surface and the depths 10, 30, 50 and 100 μm

TIME-STEP= 1636    TIME=16.360[ms]  
PROJ. POSITION=3.560[m], PROJ. VEL.= 202.3[m/s]

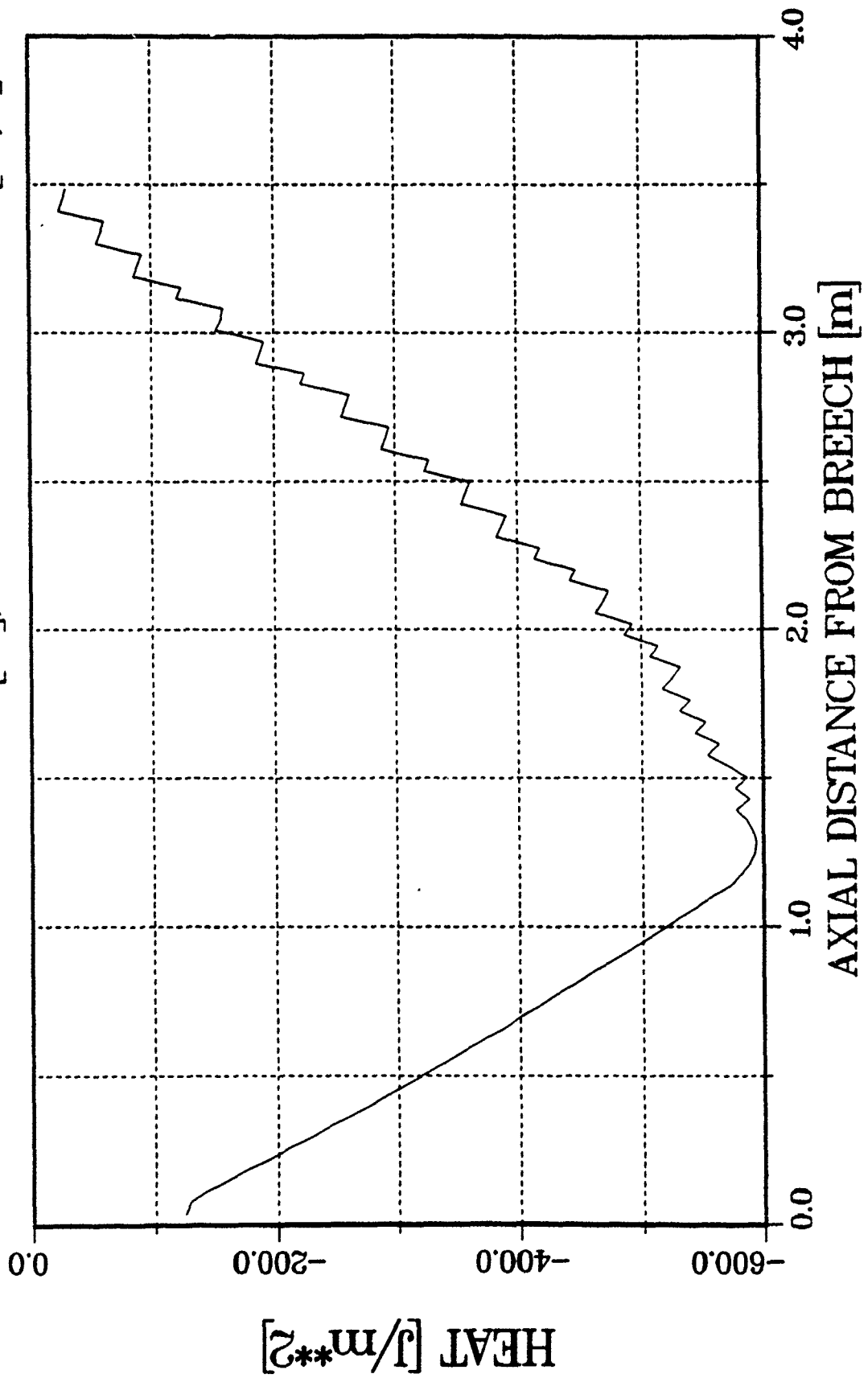


Fig. 41: Amount of heat transferred from the wall to the gas flow

A P P E N D I X

INTERIOR BALLISTICS  
AND  
GUN BARREL HEAT TRANSFER

Development of DELTA-Code Considering  
Unsteady Heat Conduction

Dr.-Ing C. S. Kocaaydin

9.10.1991

## **1. Outline**

The purpose of this research project was to develop a gun barrel heat transfer model in order to predict the thermal boundary layer development and the heat load to the barrel. This problem was actually embedded into the development of a general computer code in order to analyse the overall interior ballistics cycle in detail.

During the period from June 90 to November 90, the major research activity was concentrated on the development of a new method to consider the heat-transfer to the gun wall. The theoretical aspects of this new method have been documented already in the last report /1/. In this final report, we are going to summarize the progress achieved in the research project during the period from December 90 to September 91.

## **2. Experience with the DELTA program**

The development of a gun-barrel heat transfer model and its implementation into the DELTA code encountered several difficulties due to the numerical stability problems. This situation has led to some work, which was initially not considered.

### **2.1 Numerical Instability**

Due to the central differences and excessive quasi-linearization used within the discretization methodology of the DELTA code, this program cannot be considered as robust. Therefore, it is always necessary to adapt carefully the grid and the time-step for every initial condition. Otherwise, the results are suffering from some high-frequency oscillations. On the hand, to combine the DELTA program with a new boundary algorithm has made the stability range narrower. The computation of thermal boundary layer leads to high gradients in temperature distribution within the computation domain. So we have encountered some basic problems during this research period.

As it is well known, the remedy to the instability is some sort of artificial viscosity. Due to the basic formulation, which is currently applied in the DELTA code, it is necessary to put explicit and implicit artificial viscosity. Although the range of explicit viscosity terms are bounded upwards, there is actually no limit given to the implicit artificial terms. After several tests have been run with the DELTA code, it was confirmed, that the DELTA code doesn't react stable if the coefficient of implicit artificial viscosity is increased. It is recommended to consider some recent publications on the role of artificial viscosity /2/.

After a rigorous control of the program, it was found that this above mentioned phenomenon is a result of an error in the implementation of implicit artificial viscosity. Let's consider the linearized block implicit scheme used in the DELTA code. Complete description of the method can be found in /3,4/.

The general form of the governing nonlinear partial differential equation is

$$\frac{dy}{dt} = G(r, z, t, y, y_r, y_z, y_{rr}, y_{rz}, y_{zz}) \quad (1)$$

where the independent variables of time, radial and axial coordinates are denoted by  $t, r, z$ , respectively. The vector of dependent variables is denoted by  $y$ . The alternating direction - implicit method (ADI) used in DELTA is

$$\begin{aligned} [I - \beta D_r^n] y^I &= [I - \beta D_r^C] y^C + Ly^C \quad , \\ [I - \beta D_z^n] y^n &= [I - \beta D_z^C] y^C + (y^I - y^C) \quad . \end{aligned} \quad (2)$$

The operator matrices  $D_r$  and  $D_z$  have the following structure

$$\begin{aligned} D_r &= D_r (D, DR, DRR) \quad , \\ D_z &= D_z (DZ, DZZ) \quad , \end{aligned} \quad (3)$$

with the Jacobian matrices

$$D = \frac{\partial G}{\partial y} \quad , \quad DR = \frac{\partial G}{\partial y_r} \quad , \quad DRR = \frac{\partial G}{\partial y_{rr}} \quad , \quad DZ = \frac{\partial G}{\partial y_z} \quad , \quad DZZ = \frac{\partial G}{\partial y_{zz}} \quad .$$

In the present code, the implicit artificial viscosity terms were added to the operator matrices DRR and DZZ on each side of the equations - see subroutines SWRINT and SWZINT -. But it is only allowed to use these terms on the left implicit side.

After this error has been eliminated, the DELTA code has become really stable. It should be clear, that the use of artificial viscosity leads to non-physical diffusion. Therefore, these coefficients should be kept as low as possible.

There is another important question within the context of the stability problem. This is, how the Jacobian matrices should be computed. It is possible to compute them analytically or numerically. A definite answer to this question cannot be given at this moment.

## 2.2 Reduction of computation time

In order to reduce the computation time, it was decided to use only exact Jacobi matrices. So the algorithm was completely reconsidered. The computation of the right-hand-side and of the Jacobians has been recoded. By storing several intermediate quantities the computation time has been reduced drastically. On the other hand, due to the higher robustness of the code after the correction of the artificial viscosity, the time-steps could also be increased. Some existing subroutines were further developed to compute the Jacobians analytically even in case of turbulent flow. Unfortunately, this version of the program was not available for the DELTA code.

### 3. Development of a new boundary condition to couple the fluid flow and heat conduction within the wall

In this section, some details of the formulation will be presented. These are the choice of the grid, numerical aspects and boundary conditions

#### 3.1 Choice of the grid - Stability of heat-transfer

The most important aspect in the implementation of a coupled heat-transfer model was the question concerning the grid resolution in the gas and the wall. There were some open questions. The choice of any grid can affect the results. This uncertainty has been resolved in the following way

Actually, it is well known, that the grid should be fine enough within the boundary layer. Here, we are considering how the coupling of fluid and solid can influence the unsteady heat-transfer.

As we are primarily interested in the unsteady heat transfer, we should look carefully to the unsteady heat conduction equation, where temperature, density, specific heat capacity and thermal conductivity are denoted by  $T$ ,  $\rho$ ,  $c$  and  $k$  respectively.

$$\frac{\partial T}{\partial t} = \alpha \frac{\partial^2 T}{\partial x^2} ,$$

with thermal diffusivity  $\alpha$ , defined as

$$\alpha = \frac{k}{\rho c} .$$

The heat equation can be put into a dimensionless form through the choice of some appropriate reference values.

$$\frac{\partial \vartheta}{\partial \tau} = \frac{\partial^2 \vartheta}{\partial \eta^2} ,$$

with

$$\vartheta = \frac{T}{T_{\infty}} , \eta = \frac{x}{L} , \tau = \frac{t\alpha}{L^2} .$$

There is an order of magnitude difference in the diffusivity of steel and gas. So we should also analyse the unsteady thermal contact problem.

$$\frac{\partial T_1}{\partial t} = \alpha_1 \frac{\partial^2 T_1}{\partial x^2} ,$$

$$\frac{\partial T_2}{\partial t} = \alpha_2 \frac{\partial^2 T_2}{\partial x^2} , \quad \alpha_1 \neq \alpha_2 .$$

If the heat equation should be resolved in two different media simultaneously, the characteristic length of the domain should be chosen, such that the time-scale of the dimensionless equations should be the same.

$$\tau_1 = \tau_2 .$$

This leads to the following criteria

$$\frac{L_1}{L_2} = \sqrt{\frac{\alpha_1}{\alpha_2}}$$

So the computational domain used to determine the boundary temperature must be defined in a similar manner. Actually, this fact is also prescribed by the stability criteria of an explicit integration scheme. This aspect will be mentioned in the next section.

### 3.2 Numerical aspects of the formulation

The underlying theory for the formulation of a special boundary condition to couple the flow-field inside the gun and the heat-transfer in the gun-barrel has been previously reported /1/. But this numerical implementation has encountered several difficulties. In order to remove these problems, all numerical aspects have been reconsidered during the second half of the last period. Here we are giving a full description of the method.

#### 3.2.1. Discretisation and integration of the energy equation

To compute the temperature at the gun-wall, the energy equation should be integrated in a time-accurate manner. The computation domain covers naturally the gas flow inside the tube and the heat conduction in the gun-barrel. In order to localize the problem, it will be appropriate to make some assumptions. As long as the radial heat-transfer is stronger than the axial processes, we can ignore the axial convective and heat-flux terms in the energy equation. This assumption is true in case of high Peclet numbers. Reducing the two-dimensional problem into a radial heat-transfer problem, we can sweep along radial direction independently at each axial section.

Let's state the problem once again. We are looking to a radial heat-transfer problem and seeking only the temperature at a single point, which is the common boundary of two different media. Choosing an explicit scheme to integrate the energy equation, the computational domain will cover only a small region around the boundary point.

It should be remembered that an explicit scheme should obey some stability criteria. In this case the time step has been already prescribed through the solver for the fluid-dynamics problem. So we have to define the integration domain around the boundary point carefully. It is well known, that the stability criteria of an explicit scheme for a diffusion equation is given like

$$\alpha \frac{\Delta t}{\Delta x^2} \leq \frac{1}{2}$$

So we have to consider the gas and wall sides independently. Due to the different material constants, there is an order of magnitude difference in the heat diffusion coefficient. This is an essential point for the coupling of two media. It should be remembered that the diffusion coefficient depends also on temperature. That's why it is appropriate to use an auxiliary grid within this boundary algorithm. Otherwise, it is a hopeless task to find an appropriate grid to fulfill all of the requirements before running the program.

Actually we are going to formulate a three-point explicit scheme for the integration of the energy equation, which is discretized according to finite-volume method. Considering the same stability-criteria, we compute the location of a northern node N in the wall and of a southern node S in the gas. The boundary node is described by the letter P. The next step is the computation of all state variables at this new defined points. A simple interpolation is good enough for our purposes here.

$$\Delta r_{PN} = \sqrt{2 \Delta t \alpha_{\text{wall}}} \quad .$$

$$\Delta r_{PS} = \sqrt{2 \Delta t \alpha_{\text{gas}}} \quad .$$

The radial coordinate  $r_P$  of the boundary point P is defined by the geometry of the gun barrel.

$$r_N = r_P + \Delta r_{PN} \quad .$$

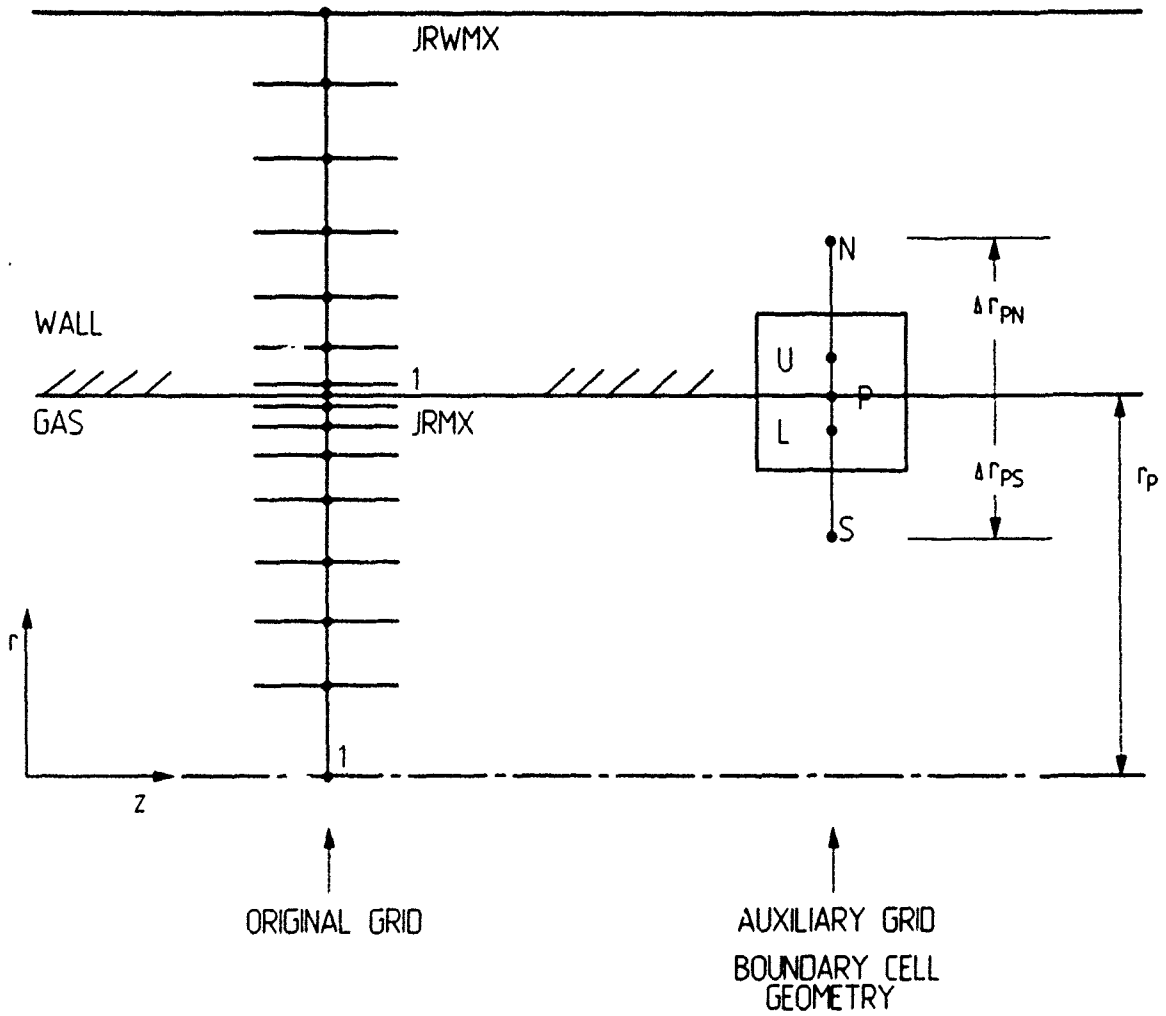
$$r_S = r_P - \Delta r_{PS} \quad .$$

Due to the difference in material constants, we cannot consider a single composite-cell at the boundary. Therefore we should define a boundary cell for each medium. The upper cell U is the boundary cell in the gun-wall. The lower cell L is just the opposite, boundary cell in the gas. An important aspect of the chosen finite-volume formulation is that we are going to make an energy balance for each boundary cell. After computing the temperature of cell centers at the new time level, the temperature of the boundary point will be determined assuming an equilibrium of heat fluxes.

The temperature at each boundary cell  $T_U$  or  $T_L$  depends directly on the boundary temperature  $T_P$ , but they are not the same. At every time-step, the state variables at the center of each boundary cell is defined through a weighted averaging of the adjacent nodes. The weighting factors are given just through geometric considerations. If we define a cell center for each boundary cell, so the location can be computed simply as given below.

$$r_U = r_P + \frac{1}{4} \Delta r_{PN} \quad .$$

$$r_L = r_P - \frac{1}{4} \Delta r_{PS} \quad .$$



According to this definition, it is also a simple arithmetic to define the weighting factors.

$$T_u = \frac{1}{4} (3T_P + T_N) \quad .$$

$$T_L = \frac{1}{4} (3T_P + T_S) \quad .$$

Let us summarize the discretization of energy equation in radial direction at each axial section. We are considering now only two cells U and L with temperatures  $T_U$  and  $T_L$ . The simplified energy equation is given below, using the common notation for finite-volume methods.

$$\begin{aligned} & \frac{c_v V}{\Delta t} \left[ (\rho T)^{n+1} - (\rho T)^n \right] + \left[ (\rho T v_r F)_N - (\rho T v_r F)_S \right] \\ & = - \left[ q_N - q_S \right] - \left[ (\rho v_r F)_N - (\rho v_r F)_S \right] + \Phi V \quad . \end{aligned}$$

The discretized equations for a radial heat-transfer sweep at an axial section are given below using the same terminology. Temperature  $T$  and density  $\rho$  will be computed at the new time level  $t^{n+1}$ . So they are unknowns in this formulation. All other variables as  $v$ ,  $p$ ,  $c_v$  will be taken from the latest available time level  $t^n$ .

Energy balance in the upper boundary cell U:

Assuming the density of the gun wall is constant, the only unknown at the upper cell is temperature.

$$\begin{aligned} & \frac{c_u \rho V_u}{\Delta t} \left[ T_u^{n+1} - T_u^n \right] \\ & = - \left[ \left( - \frac{k_{PN}}{\Delta r_{PN}} (T_N^n - T_P^n) \right) F_{PN} - \left( (q_r)_P + q_{rad} \right) F_P \right] \quad . \end{aligned}$$

Energy balance in the lower boundary cell L:

In the gas, the density depends on temperature and pressure. We assume that the pressure changes can be neglected for a single time-step. So the density will be a function of temperature. The following state-law for a Nobel-Abel type gas should be considered.

$$\rho = \frac{1}{\frac{RT}{MP} + \eta}$$

$$\begin{aligned} & \frac{c_v V_L}{\Delta t} \left[ (\rho T)_L^{n+1} - (\rho T)_L^n \right] + \left[ - (v_r)_{PS} F_{PS} (\rho T)_{PS}^n \right] c_v \\ & = - \left[ (q_r)_P F_P - \left( - \frac{k_{PS}}{\Delta r_{PS}} F_{PS} (T_P^n - T_S^n) \right) \right] - \left[ - (v_r)_{PS} F_{PS} p_{PS} \right] + \Phi_L V_L \end{aligned}$$

This nonlinear equation can be easily solved by a damped Newton method.

Finally we should define the heat-flux at the boundary  $q_p$ , so that the equations can be integrated explicitly. For this purpose, we assume a local equilibrium of heat-flux between the wall and gas. Using the same terminology, this means that the heat-flux from the cell center L towards the boundary point P is equal to the heat-flux from the boundary point P towards the upper cell center U. It is easy to define the heat-flux in the solid, because heat conduction is the only heat-transfer mechanism. On the other hand, it is very difficult to describe the heat-flux through a fluid layer at the wall. Considering the following relation according to the local equilibrium

$$q_p = q_{\text{wall}} = q_{\text{gas}}$$

the heat flux is defined simply using the information on the solid side

$$q_p = - \frac{T_U^n - T_P^n}{\frac{\Delta r_{PN}}{4k_{PN}}}$$

### 3.2.2 Determination of surface temperature

After the equations have been solved for temperature of cell centers at the new time level, the final step will be to determine the new temperature at the boundary. We have already assumed that there is an equilibrium of heat-fluxes within each medium at the boundary. Since we have considered the unsteadiness of the problem and also taken account of all the convective terms, this assumption can be justified.

In order to make the details clear, we should look at first to a simple contact problem. Let's consider the contact of two solid layers ( upper and lower ) having different heat-conductivity  $k_{PN}$  and  $k_{PS}$  respectively. The thickness of the layers will be described by  $\Delta r_{PN}$  and  $\Delta r_{PS}$ . In this case, heat conduction is the only heat-transfer mechanism. Finally this composite layer should be held between a temperature difference  $T_U$  and  $T_L$ . The boundary temperature between two solid layers can be computed considering an equilibrium of heat-flux using the following equation

$$T_P^{n+1} = \frac{\frac{\Delta r_{PN}}{k_{PN}} \cdot T_u^{n+1} + \frac{\Delta r_{PS}}{k_{PS}} \cdot T_L^{n+1}}{\frac{\Delta r_{PN}}{k_{PN}} + \frac{\Delta r_{PS}}{k_{PS}}}$$

Actually this relationship cannot be used in case of contact between a solid and fluid layer. The reason is that the heat-flux on the fluid side is not only due to the heat-conduction. However we can use the already available information on the velocity distribution near to the wall in order to define the wall heat-flux on the fluid side. This is to say that the method of solution

is an analogy between the velocity and temperature distribution sometimes known as the Reynolds-analogy. In case of high-speed flows having a Prandtl number close to one, this assumed similarity between velocity and temperature distribution is reasonable.

At this point it is important to note that we are going to use the Reynolds-analogy only in the boundary cell which we have already discussed. The velocity gradient at the wall is evaluated on the original grid.

$$\begin{aligned} q_p &= -k_{PS} \left. \frac{\partial T}{\partial r} \right|_w \\ &= -k_{PS} \left. \frac{\partial T}{\partial u} \frac{\partial u}{\partial r} \right|_w = -k_{PS} \frac{(T_S^n - T_P^n)}{u_S} \left. \frac{\partial u}{\partial r} \right|_w \end{aligned}$$

So we can define a heat-transfer coefficient  $\alpha_{PS}$ .

$$\alpha_{PS} = \frac{q_p}{(T_P^n - T_L^n)}$$

Finally the wall temperature can be computed similarly.

$$T_P^{n+1} = \frac{\frac{\Delta r_{PN}}{k_{PN}} \cdot T_u^{n+1} + \alpha_{PS} T_L^{n+1}}{\frac{\Delta r_{PN}}{k_{PN}} + \alpha_{PS}}$$

### 3.2.3 Influence of grid-motion on the wall temperature

Up to now, we have considered the heat-transfer within a stationary grid system. Therefore the wall temperature should be modified concerning the grid motion. This is accomplished through a simple interpolation of the wall temperature using the old grid and computing the temperature at the new grid points along the wall. Concerning the wall/base corner point special care is necessary. Due to the projectile motion, the grid is expanding. The regions which are entering the computational domain are assumed to be at the room temperature. But this is not valid for the wall points, except the wall/base corner point. Due to the strong expansion of the grid, it can happen that some wall points will be between the old and new projectile locations. Therefore we have to compute the temperature of the wall/base corner point belonging to the old grid at the new time level. This value is used here only for internal purposes during interpolation of wall temperature. It will be helpful to compare with the details of boundary conditions in section 3.4 .

### 3.3 Discussion of the new boundary algorithm.

The presented formulation has the aim to consider the unsteady and convective nature of the heat-transfer problem at the boundary of a fluid and solid. It has been observed, that a further assumption in order to simplify the problem can be made. This is that the radial convection and the pressure work terms can be neglected, if the radial velocity is truly vanishing. This is not always the case. Even some very small radial velocity leads to very high radial convection and pressure work, because both of the state variables temperature and pressure attain very high magnitudes. Within the context of stability, this phenomenon causes also trouble. Remember that we are using only a one-step explicit scheme. So it may be better, to use a fine grid at the boundary and neglect these terms as long as an explicit scheme is used.

So the simplified energy equation describes the unsteady temperature distribution in a Couette-flow, balancing the heat conduction with the heat-generation through viscous dissipation. Actually all universal wall-functions have originated from such models.

### 3.4 Modification of Boundary Conditions

The definition of boundary conditions is usually considered as the most important aspect of a numerical simulation program. Therefore, special attention is required.

In order to make the DELTA code transparent, the subroutines concerning boundary conditions have been simplified. Concerning the momentum equation, no-slip condition is used everywhere except the base, where the velocity is prescribed. At the breech the axial pressure gradient and along the wall the radial pressure gradient is set to zero. Along the axis the symmetry condition is well defined.

For the gasdynamical problem in an interior ballistics cycle with a coupled gun-barrel heat-transfer modelling, the boundary conditions at the base of the projectile were modified. It has been observed that the thickness of the thermal boundary-layer is unrealistically big behind the projectile base. Therefore a correction of pressure and entropy is necessary. The flow at the base has been assumed as one-dimensional. After every time-step, the pressure and entropy along the base of the projectile were set equal to corresponding values at the axis. It should be mentioned, that the grid is uniform in the axial direction. That's why the resolution of any viscous flow phenomena at the base cannot be achieved.

One important detail belongs to the handling of the wall/base corner point. Actually, there are at least two different states at this singular point. If we consider, that this point belongs to the wall, its velocity is set to zero. Concerning the entropy, the situation is somewhat different. This singular point is also the edge of the boundary-layer. If we assume that the boundary

layer has not been developed, then we can define the temperature of this point through extrapolation from the gas flow. On the other hand, if we are going to compute the heat conduction within the gun-barrel, we should remember that the heat-flux has not entered into the wall yet. So we should consider that this singular point is still at room temperature.

#### **4.0 Discussion of numerical results and conclusion**

The gun-barrel heat-transfer is controlled through convective and viscous processes within boundary layer. At the beginning of the ballistic cycle, the wall temperature close to the base of the projectile attains very high values. This peak is caused through the developing boundary layer. At the edge of the boundary-layer the viscous dissipation is very high. Beside that the hot gas of the core-flow touches instantaneously the wall/base corner point.

Another important process is the radial convection behind the projectile base. The axial velocity of the gas behind the projectile is larger than the projectile velocity. Due to the deceleration of the gas flow behind the projectile, there is a change of flow direction from axial towards radial. So the heat load is further increased through radial convection. It should be remembered this deceleration process is also an adiabatic heating. The flow-field behind the projectile is a combination of two completely different phenomena. The adiabatic heating is reacting against the expansion flow due projectile motion.

Concerning the numerical simulation of interior ballistics, there is still some need for the development of an efficient method. The DELTA code is actually describing the hydrodynamics of the problem. Even for this problem, it will be appropriate to rewrite the code. Using the same theoretical modelling with a modern implicit discretisation method, based on upwind finite differences and considering an efficient code-structure, this task can be fully achieved in a reasonable short time.

#### **5. References**

- /1/ Kocaaydin, C.S., Interior ballistics and gun-barrel heat-transfer, Mid-term report for the contract of EMI-AFB, submitted within the sixth periodic report, 1990
- /2/ Mahajan, A.J., Dowell, E.H., Bliss, D.B., Role of artificial viscosity in Euler and Navier-Stokes Solvers, AIAA J., 29, 1991, 555-559
- /3/ Schmitt, J.A., A numerical algorithm for the multidimensional, multi-phase, viscous equations of interior ballistics, Trans. of the sec. Army Conf. on Appl. Math. and Comp., ARO Report 85-1, p.649-691, 1985
- /4/ Heiser, R., Schmitt, J.A., Simulation of special interior ballistic phenomena with and without heat transfer to the gun tube wall, Trans. of the sec. Army Conf. on Appl. Math. and Comp., ARO Report